

1 **Variscan structures and their control on latest to post-Variscan basin architecture; insights from**
2 **the westernmost Bohemian Massif and SE Germany**

3
4 **Hamed Fazlikhani, Wolfgang Bauer and Harald Stollhofen**

5
6 GeoZentrum Nordbayern, Friedrich-Alexander-Universität (FAU) Erlangen-Nürnberg, Schlossgarten 5
7 5, 91054 Erlangen, Germany.

8 *Correspondence to: Hamed Fazlikhani (hamed.fazli.khani@fau.de)*

9 **Abstract**

10 The Bohemian Massif exposes structures and metamorphic rocks remnant from the Variscan Orogeny
11 in Central Europe and is bordered by the Franconian Fault System (FFS) to the west. Across the FFS,
12 Variscan units and structures are buried by Permo-Mesozoic sedimentary rocks. We integrate existing
13 DEKORP 2D seismic reflection, well and surface geological data with the newly acquired FRANKEN 2D
14 seismic survey to investigate the possible westward continuation of Variscan tectonostratigraphic
15 units and structures, and their influence on latest to post-Variscan basin development. Subsurface
16 Permo-Mesozoic stratigraphy is obtained from available wells and tied to seismic reflection profiles
17 using a synthetic seismogram calculated from density and velocity logs. Below the sedimentary cover,
18 three main basement units are identified using seismic facies descriptions that are compared with
19 seismic reflection characteristics of exposed Variscan units east of the FFS. Our results show that upper
20 Paleozoic low-grade metasedimentary rocks and possible Variscan nappes bounded and transported
21 by Variscan shear zones ca. 65 km west of the FFS. Basement seismic facies in the footwall of the
22 Variscan shear zones are interpreted as Cadomian basement and overlying Paleozoic sequences. We
23 show that the location of normal fault-bounded latest to post-Variscan late Carboniferous-Permian
24 basins are controlled by the geometry of underlying Variscan shear zones. Some of these late
25 Carboniferous-Permian normal faults reactivated as steep reverse faults during the regional Upper
26 Cretaceous inversion. Our results also highlight that reverse reactivation of normal faults gradually
27 decreases west of the FFS.

28 **1. Introduction**

29 Variscan orogenic units and structures in central and western Europe are extensively studied from
30 disconnected exposed terranes in the Bohemian Massif, the Rheno-Hercynian Massif, the Black forest
31 and Vosges, the Armorican Massif and the Central Iberian Zone (Franke, 2000). Between exposed
32 Variscan units, younger sedimentary rocks obscure direct observation of possible lateral extension
33 and architecture of Variscan tectonostratigraphy and structures. In southern Germany, for instance,
34 Variscan units of the Bohemian Massif are correlated with exposed Variscan units in the Black Forest
35 and Vosges, ca. 300 km apart from each other, causing uncertainties in the lateral continuation and
36 architecture of the Variscan tectonometamorphic Saxothuringian and Moldanubian zones, originally
37 defined by (Kossmat, 1927). Although a few wells provide local but valuable information about
38 basement rock types, only a few regional 2D seismic profiles (DEKORP 84-2s and 90-3B/MVE and
39 KTB84) image the Variscan units and structures below the sedimentary cover between the Bohemian
40 Massif and Black Forest exposures (Franke et al., 2017; Behr and Heinrichs, 1987; Wever et al., 1990;
41 Edel and Weber, 1995; Meissner et al., 1987; Lüschen et al., 1987).

42 The recently acquired FRANKEN 2D seismic survey covers the Carboniferous-Permian Kraichgau and
43 Naab basins (Paul and Schröder, 2012; Sitting and Nitsch, 2012) and the overlying late Permian to
44 Triassic Franconian Basin (Freudenberger and Schwerd, 1996) in the western vicinity of Bohemian
45 Massif in SE Germany (Fig. 1). The FRANKEN survey is tied to the DEKORP 3/MVE-90 profile creating a

46 grid of regional seismic reflection profiles imaging exposed and buried Saxothuringian units and
47 structures of the Variscan Orogeny across the Franconian Fault System (FFS, Fig. 1). In this study we
48 investigate the potential westward extension of Variscan tectonic units and structures and construct
49 a first order relationship between Variscan and post-Variscan structures and basin development. Four
50 new seismic profiles of the FRANKEN survey are interpreted utilizing subsurface and surface geological
51 data and are tied to the existing DEKORP-3/MVE-90 profile. Underneath the Permo-Mesozoic
52 sedimentary cover three main Basement Seismic Facies (BSF1-3) are identified, based on lateral and
53 vertical changes in reflection amplitude and connectivity. Comparing seismic reflection patterns
54 observed in exposed Variscan rocks of Bohemian Massif with reflection patterns along the FRANKEN
55 seismic profiles we show a W-SW continuation of Variscan shear zones and associated Variscan
56 allochthons. The control of Variscan shear zone geometry in strain localization and latest to post-
57 Variscan basin development and brittle fault interactions are discussed.

58 **2. Geological setting**

59 **2.1. Variscan geodynamics and tectonic framework**

60 The Bohemian Massif comprises remnants of the Upper Paleozoic collision of Laurussia and
61 Gondwana, known as Variscan Mountain Belt, and of the pre-Variscan basement in Central Europe
62 (Franke, 2000; Kroner et al., 2007). The Variscan Orogeny has produced a wide range of metamorphic
63 units, ranging from high-pressure and high-temperature metamorphic to low-grade metasedimentary
64 rocks, abundant granitic intrusives and crustal-scale shear zones and faults. From north to south, the
65 Variscides have traditionally been subdivided into three main tectonometamorphic zones, the
66 Rhenohercynian, Saxothuringian (including the Mid-German Crystalline High) and Moldanubian
67 (Kossmat, 1927; Franke, 2000; Kroner et al., 2007). Saxothuringian and Moldanubian rocks are well
68 exposed in the Bohemian Massif, but buried by Paleozoic and Mesozoic sediments towards the west.

69 The Saxothuringian zone and its westward extension, as the main area of interest, underwent three
70 main deformational phases during the Variscan Orogeny (Kroner et al., 2007 and references therein).
71 A first deformation phase (D1) developed before 340 Ma and records pervasive deformation during
72 the subduction and collision resulting in the development of recumbent folds and thrusts with top-to-
73 the-southwest transport direction as evidenced by kinematic indicators (Kroner et al., 2007; Stettner,
74 1974; Franke et al., 1992; Schwan, 1974). A second deformation phase (D2) developed due to the
75 exhumation and juxtaposition of High-pressure and Ultra high-pressure metamorphic rocks in the
76 upper crust and a ca. 45° rotation in principal subhorizontal compression direction to NNW-SSE after
77 340 Ma (Kroner and Goerz, 2010; Schönig et al., 2020; Hallas et al., 2021; Stephan et al., 2016). The
78 D2 deformation phase is manifested by dextral transpression of D1 structures and ductile deformation
79 with a generally top-to-the-northwest transport direction (Kroner et al., 2007; Franke and Stein, 2000;
80 Kroner and Goerz, 2010; Franke, 1989). A third deformation phase (D3) records latest Variscan
81 tectonics at ~320 Ma and is represented by the folding of synorogenic deposits during general NW-SE
82 to NNW-SSE shortening (Hahn et al., 2010). Latest stages of D3 and early post-Variscan is dominated
83 by a wrench tectonic phase and the collapse of thickened crust, resulting in the development of dextral
84 strike-slip faults initiating fault-bounded graben and half-graben basins in Central Europe, including
85 the study area in SE Germany (Schröder, 1987; Arthaud and Matte, 1977; Krohe, 1996; Stephan et al.,
86 2016; Peterek et al., 1996b; Ziegler, 1990; Eberts et al., 2021). Detailed and comprehensive overviews
87 of the geodynamic and tectonostratigraphic evolution of the Mideuropean Variscides have been
88 presented by (Linnemann and Romer, 2010; Franke et al., 2000).

89 During earliest post-Variscan development at <305 Ma, wide-spread intermontane Late
90 Carboniferous-Permian fault bounded graben and half-graben basins, such as the NE-SW trending
91 Saar-Nahe (Henk, 1993; Stollhofen, 1998; Boy et al., 2012) Saale (Ehling and Gebhardt, 2012),
92 Kraichgau and Schramberg basins (Sitting and Nitsch, 2012) and NW-SE striking basins (e.g. Naab and
93 Thuringian Forest basins) are formed (Paul and Schröder, 2012; Lützner et al., 2012). The Rotliegend

94 is characterized by widespread intrabasinal volcanism and depositional areas became enlarged across
95 the internal parts of the Variscan Belt, e.g. in Switzerland (Matter et al., 1987), France (Chateauneuf
96 and Farjanel, 1989; Cassinis et al., 1995; Engel et al., 1982; Laverranne, 1978; McCann et al., 2006),
97 Germany (Henk, 1993; Stollhofen, 1998; Boy et al., 2012; Lützner et al., 2012; Sitting and Nitsch, 2012;
98 Paul and Schröder, 2012) and Iberia (e.g. (Cassinis et al., 1995). In the study area, Carboniferous-
99 Permian units are only exposed along the Franconian Fault System (FFS, also known as Franconian
100 Line), but have been drilled by several wells located farther west, in the Kraichgau and Naab basins
101 (Fig. 1, Table 1).

102 In general, the top of Saxothuringian basement units beneath the sedimentary cover shows a smooth
103 topography with a gentle southward rise, including lows along the SW-NE axis Würzburg-Rannungen
104 and along the NW-SE axis Staffelstein-Obernsees, the latter subparallel to the FFS (Gudden, 1981;
105 Gudden and Schmid, 1985). Saxothuringian basement lithologies drilled by wells Wolfersdorf and
106 Mittelberg in the north, well Eltmann to the west and well Obernsees in the southeast of the study
107 area (Fig. 1 and Table 1) are Upper Devonian to lower Carboniferous low to medium-grade
108 metasedimentary rocks (Hahn et al., 2010; Stettner and Salger, 1985; Trusheim, 1964; Specht, 2018;
109 Friedlein and Hahn, 2018).

110 **2.2. Latest to post-Variscan stratigraphic and structural architecture**

111 Carboniferous-Permian units in the study area dominantly comprise clastic continental sediments
112 deposited in fault-bounded basins outcropping in the Schalkau, Stockheim, Rugendorf, Wirsberg and
113 Weidenberg areas (Schröder, 1987). Thicknesses are highly variable, ranging from about 100 m to
114 >700 m in the Kraichgau Basin and from about 100 m up to >1400 m in the Naab Basin adjacent to the
115 FFS (Gudden, 1981; Paul and Schröder, 2012). In Stockheim outcrop, well Wolfersdorf drilled into 726
116 m Rotliegend, excluding an unknown amount of eroded section (Fig. 1 and Table 1). In the center of
117 the study area, 109 m of Rotliegend were encountered by well Mürsbach 1 (Gudden, 1981), whereas
118 wells Mürsbach 6 and Staffelstein 1 only penetrated ca. 20 and 43 m into the upper parts of the
119 Rotliegend (Table 1). Well Eltmann, located in a basin marginal position, encountered only 3 m
120 Rotliegend (Table 1, (Trusheim, 1964). Towards the SE of the study area well Obernsees encountered
121 18.3 m of Rotliegend overlying metasedimentary basement rocks (Table 1, (Helmkamp, 2006; Ravidà
122 et al., 2021). However, ca. 19 km NE of well Obernsees, well Lindau 1 drilled 250.25 m of Rotliegend
123 strata without reaching their base (Fig. 1, Table 1; (Freudenberger et al., 2006). Compared to the
124 Rotliegend, the Zechstein tends to be of more uniform thickness mainly comprising of clay- and
125 sandstones, dolomites and thin layers of anhydrite (Schuh, 1985). Drilled Zechstein thicknesses are
126 117 m in well Eltmann, 126 m in well Mürsbach 1, and 107 m in well Staffelstein and 104.9 in well
127 Obernsees (Table 1). Refraction seismic surveys in the south of the study area (Nürnberg area) proved
128 the existence of deep, fault-bounded grabens, whereas the Rotliegend top is characterized by a
129 peneplain beneath the Zechstein (Bader and Bram, 2001; Bunn and Bram, 2001). This suggests a
130 regional unconformity between Rotliegend and Zechstein and supports the separation between the
131 Carboniferous-Permian (mainly Rotliegend) Kraichgau Basin and the post-Rotliegend (mainly
132 Mesozoic) Franconian Basin development (Freudenberger et al., 2006; Paul, 2006).

133 Triassic stratigraphy is divided into Lower to lowermost Middle Triassic Buntsandstein, the Middle
134 Triassic Muschelkalk and the uppermost Middle to Upper Triassic Keuper Groups (STD, 2016; Fig. 2).
135 Siliciclastic sandstones of the Buntsandstein Group are 572 m thick in well Staffelstein 1, 530.7 m in
136 well Mürsbach 6, and 510 m in well Eltmann, decreasing to 417.15 m in well Obernsees in the
137 southeast (Table 1, (Gudden, 1977; Emmert et al., 1985; Helmkamp, 2006). Buntsandstein units are
138 exposed in fault blocks between the FFS and the Eisfeld-Kulmbach fault in the eastern part of the study
139 area (Fig. 1). The Muschelkalk Group is dominated by carbonates, dolomites and few gypsum, 240 m
140 thick in well Staffelstein 1, 210.7 m in well Mürsbach 6, and 236 m in well Eltmann, decreasing

141 southeastward to 178 m in well Obernsees (Table 1, (Gudden, 1977; Emmert et al., 1985). Muschelkalk
142 units crop out along the FFS and the Eisfeld-Kulmbach fault and also west of well Eltmann (Fig. 1). The
143 Keuper Group consists mainly of sandstones that are 530.2 m thick in well Staffelstein 1, 532 m in well
144 Staffelstein 2, decreasing southeastward to 483 m in well Obernsees (Franz et al., 2014; Gudden, 1977;
145 Emmert et al., 1985). Keuper units are broadly exposed in the western and northwestern part of the
146 study area and in the fault block bounded by the Eisfeld-Kulmbach and Asslitz faults (Fig. 1). Jurassic
147 units preserved in the central and eastern parts of the study area, but eroded towards the west and
148 northwest (Fig. 1). Jurassic outcrops to the east are fault bounded and are limited to the footwall of
149 Eisfeld-Kulmbach, Asslitz and Lichtenfels reverse faults (Fig. 1). The Jurassic interval is 102 to 104 m
150 thick in wells Staffelstein 1 & 2 in the north and 140 m thick in well Obernsees in the SE (Table 1;
151 Meyer, 1985; Gudden, 1977). Cretaceous sedimentary rocks are preserved in the central and
152 southeastern parts of the study area (Fig. 1).

153 The structural architecture of the eastern study area is characterized by ten to hundreds of kilometer
154 long NW-SE striking multi-segmented reverse faults (e.g. Eisfeld-Kulmbach and Asslitz faults), whereas
155 towards the west only normal faults (e.g. Bamberg Fault, Kissingen-Haßfurt fault zone) are developed
156 (Fig. 1). The NW-SE striking Franconian Fault System (FFS) is the dominant structural feature,
157 representing the tectonic contact between the western Bohemian Massif to the east and the late
158 Permian to Mesozoic Franconian Basin to the west (Fig. 1). The FFS initiated most likely during latest
159 Variscan tectonics and was reactivated at least during Early Triassic and Cretaceous times (Carlé, 1955;
160 Freyberg, 1969; Peterek et al., 1997; Wagner et al., 1997). The total amount of hangingwall uplift on
161 the FFA is estimated at ca. 5500 m, as evidenced by titanite and apatite fission-track ages, the sericite
162 K-Ar ages of fault rocks and the sedimentary strata adjacent to the fault (Wemmer, 1991; Wagner et
163 al., 1997; Peterek et al., 1997). Sub-parallel to and ca. 9 km SW of the FFS, the NE dipping Eisfeld-
164 Kulmbach Fault mainly exposes Lower and Middle Triassic units on its hangingwall side (Fig.1). In the
165 SE and the central footwall of the Eisfeld-Kulmbach Fault, Upper Triassic and Lower Jurassic units crop
166 out, while laterally to the NW Lower and Middle Triassic and some Permian units (Schalkau outcrop)
167 are exposed (Fig.1). Farther SW in the footwall of Eisfeld-Kulmbach Fault, the Asslitz Fault can be
168 traced over ca. 50 km, exposing Upper Triassic units in its hanging wall (Fig. 1). The westernmost major
169 reverse fault is the Lichtenfels Fault, mapped over ca. 16 km at the surface (Fig. 1).

170 West and southwest of the Lichtenfels Fault, the structural architecture of the study area is dominated
171 by NW-SE normal faults such as the Staffelstein and Bamberg faults and the prominent Kissingen-
172 Haßfurt fault zone (Fig. 1). Studies of regional upper crustal paleostress patterns reveal multiple
173 changes in stress field orientations since the Palaeozoic comprising normal faulting and both,
174 extensional and compressional strike-slip faulting implying multiple fault reactivation events (Peterek
175 et al., 1996a; Peterek et al., 1997; Bergerat and Geysant, 1982; Coubal et al., 2015; Navabpour et al.,
176 2017; Köhler et al. submitted).

177 **3. Data and methods**

178 **3.1. FRANKEN seismic reflection acquisition and recording parameters**

179 The FRANKEN 2D seismic survey comprises of four seismic lines, with a total line length of 230.8 km.
180 The survey area is situated in northern Bavaria, SE Germany covering an area of approximately 90 km
181 x 45 km (Fig. 1). The FRANKEN seismic survey was designed to cross deep wells and image the upper
182 crustal levels in northern Bavaria. Together with existing DEKORP, KTB and OPFZ it constitutes a grid
183 of 2D seismic reflection profiles, crossing major structural elements. FRANKEN-1801 and 1803 lines
184 are striking NW-SE perpendicular to FRANKEN-1802 and 1804 profiles (Fig. 1). Profile FRANKEN-1803
185 links to the DEKORP-3/MVE-90 profile in the NW and to the OPFZ-9301 profile towards the SE (Fig. 1).

186 FRANKEN-1802 and 1804 strike NE-SW and are perpendicular to the major fault zones. Table 2
187 summarizes acquisition and processing parameters of the FRANKEN seismic survey.

188 **3.2 Seismic interpretation methods**

189 In this study we integrate information from 9 deep wells (1100-1600 m) and surface geology to
190 interpret the newly acquired FRANKEN seismic reflection survey in SE Germany. Available wells are
191 mainly located in the center and the western part of the study area (Fig. 1 and Table 1). Seismic-well
192 tie and time-depth relationships are established using sonic velocity and density logs of the Mürsbach
193 1 well (Gudden, 1971). The calculated synthetic seismogram is correlated with the real seismic traces
194 at the well location and enabled us to transfer geological, in particular stratigraphic information from
195 the well to the intersected seismic profiles (Fig. 2). Horizon interpretation started from the profile
196 FRANKEN-1802 at the well Mürsbach-1 location where the best seismic-well tie has been established.
197 Interpretation of stratigraphic markers was then extended from the profile FRANKEN-1802 to other
198 intersecting profiles. In the sedimentary cover, seismo-stratigraphic facies and seismic characters are
199 defined, based on the lateral and vertical changes in seismic amplitudes, reflectivity and coherency.
200 Observed formation tops in wells in combination with defined seismo-stratigraphic facies are used in
201 the seismic horizon interpretation especially where there is no well available. Below the sedimentary
202 cover three main seismic facies are identified and are used to characterize and interpret basement
203 units.

204 **3.3 Seismo-stratigraphic facies**

205 Characteristic seismic signatures of stratigraphic intervals drilled by wells and observed in the
206 FRANKEN survey are first described for the Permo-Mesozoic interval. Upper Mesozoic-Cretaceous
207 units are only locally preserved in the study area and are not drilled by any of the deep wells,
208 restricting the interpretation of the Jurassic-Cretaceous boundary and the description of their seismic
209 signature. Jurassic strata show a medium amplitude and semi-continuous reflections (Fig. 3A). The
210 Triassic-Jurassic boundary is marked by the appearance of slightly higher amplitudes and rather
211 continuous reflections in the Triassic compared to the overlying Jurassic interval (Fig. 3A). This
212 boundary is correlated with the Staffelstein and Obernsees wells along profiles FRANKEN-1802 and
213 1803 respectively.

214 Upper Triassic Keuper units generally show continuous and medium to high amplitude reflections of
215 alternating sandstones, siltstones and some gypsiferous units (Fig. 3B). Only the shallow marine
216 dolomites (Grabfeld Fm.) at the base of the Keuper Group (Haunschild, 1985; Gudden, 1981) are
217 characterized by high amplitudes and continuous pairs of reflections acting as regional marker
218 reflection along all profiles (Fig. 3B). Middle Triassic Muschelkalk units are comprised of lime-, marl-,
219 and dolostones that are recorded by two distinct seismic facies in the study area, 1) a semi-continuous
220 and medium amplitude reflection with ca. 50 ms (TWT) thickness on top and 2) continuous and high
221 amplitude reflections at the bottom (Fig. 3C). The sandstone-dominated Buntsandstein Group is
222 characterized by semi-continuous and medium energy amplitudes that show gradually increasing
223 energy and continuity towards the top (Fig. 3D). A continuous and very high amplitude reflection
224 defines the Permian-Triassic boundary between the Buntsandstein and the underlying Zechstein
225 Group (Fig.3D). The latter shows ca. 25-30 ms (TWT) of continuous and high amplitude reflections
226 which are correlated to an anhydrite and dolomite bearing interval in the upper part of the Zechstein
227 (Gudden, 1977; Schuh, 1985; Gudden and Schmid, 1985). Below the Zechstein high amplitude
228 reflections, semi-continuous and medium amplitude reflections of the Rotliegend occur (Fig. 3E).
229 These reflections represent the upper parts of the Rotliegend and gradually become less distinct and
230 discontinuous with depth with some reflections being only locally present and laterally becoming less

231 pronounced to partly transparent (Fig. 3E, 4A & B). The boundary between the sedimentary cover and
232 the underlying pre-Permian low- to medium-grade metasedimentary rocks (hereafter considered as
233 basement rocks) is drilled by wells Wolfersdorf and Mittelberg in the north, Eltmann to the west and
234 the Obersees to the southeast and is not particularly reflective in the seismic survey (Table 1 and Fig.
235 4A & B). However, at some locations semi-continuous and low energy reflections of the Rotliegend
236 can be distinguished from discontinuous but slightly higher energy reflections below. When is
237 identified, such changes in reflection patterns is interpreted as the boundary between sedimentary
238 cover and underlying metasedimentary rocks (Fig. 4A & B).

239 **3.4 Basement seismic facies**

240 Basement units below the sedimentary cover comprise three seismic facies, based on observed
241 differences in reflectivity, frequency and continuity of reflections.

242 **3.4.1 Basement Seismic Facies 1 (BSF1)**

243 Basement Seismic Facies 1 (BSF1) consists of discontinuous, low amplitude and low frequency
244 reflections that become transparent at some locations (Figs. 4A & B). Higher amplitude and semi-
245 continuous reflections of the Rotliegend progressively grade into BSF1 without a seismically
246 detectable boundary (Fig. 4B). The thicknesses of BSF1 units generally decrease westward and reach
247 2.5 s TWT at their deepest position. BSF1 is sampled by well Eltmann where 94 m of (?Devonian)
248 quartzites and metasedimentary rocks are described (Trusheim, 1964), whereas well Obersees cored
249 48.3 m of ?late Paleozoic metasedimentary rocks (Table 1, Stettner and Salger, 1985). Farther north
250 well Mittelberg drilled into 100.5 m of Upper Devonian-Lower Carboniferous rocks below the
251 Rotliegend (Table 1, (Friedlein and Hahn, 2018; Hahn et al., 2010). These Upper Devonian-Lower
252 Carboniferous rocks (Gleitsch Formation) are interpreted as syn-Variscan inner shelf facies
253 sedimentary rocks (Thuringian facies), low grade metamorphosed during the Variscan Orogeny (Hahn
254 et al., 2010; Kroner et al., 2007). Although well Mittelberg is not tied to seismic profiles it additionally
255 confirms the presence of low grade metasedimentary rocks below the Rotliegend.

256 In the FFS's hangingwall, Münchberg nappe units (Variscan allochthon) are transected by the
257 DEKORP85-4N and DEKORP-3/MVE-90 seismic profiles (Figs. 1 and 5, (Hirschmann, 1996; Heinrichs et
258 al., 1994). Münchberg nappe units are surrounded by low grade metasedimentary rocks of outer shelf
259 facies (Bavarian facies) and inner shelf facies (Thuringian facies; Gümbel, 1879; Linnemann et al.,
260 2010; Heuse et al., 2010). Exposed nappe units and low grade metasedimentary rocks show
261 discontinuous to semi-continuous and low amplitude reflections, similar to BSF1 of the FRANKEN
262 survey in the FFS footwall (Fig. 5). Similar low amplitude and low frequency reflections of BSF1 are
263 also observed at the NW end of the DEKORP85-4N profile (Fig. 5A & B). There, these reflections are
264 associated with low-grade Lower Carboniferous flysch deposits (inner and outer shelf facies) exposed
265 at the surface (DEKORP Research Group, 1994a). Based on seismic facies description and in the
266 absence of well information, differentiation between allochthons, flysch sedimentary rocks, inner and
267 outer shelf facies is ambiguous. BSF1 is therefore interpreted as the western to southwestern
268 extension of low-grade inner and outer shelf facies, low-grade Lower Carboniferous flysch
269 sedimentary rocks and possible Variscan allochthons (DEKORP Research Group, 1994b). Correlating
270 with exposed basement units E-NE of the FFS, these units are interpreted to represent the W-SW
271 extension of the Ziegenrück-Teuschnitz Syncline of the Saxothuringian zone.

272 **3.4.2 Basement Seismic Facies 2 (BSF2)**

273 High amplitude, continuous and dipping reflection packages are bounding BSF1 at depth and are
274 defined as Basement Seismic Facies 2 (BSF2, Fig. 4A, C and 5). BSF2 reflections are not drilled by wells

275 within the survey area. However, similar reflections observed along reprocessed DEKORP85-4N and
276 DEKORP-3/MVE-90 profiles below BSF1 can be correlated with exposures of highly sheared rocks
277 including phyllites developed during Variscan tectonics (Fig. 5; DEKORP and Orogenic Processes
278 Working Group, 1999; Franke and Stein, 2000). We interpret BSF2 as Variscan detachment/shear
279 zones translating and involving low-grade inner and outer shelf facies, low-grade Lower Carboniferous
280 flysch sedimentary rocks and Variscan nappes. BSF2 therefore includes the upper parts of the
281 Saxothuringian parautochthons (highly sheared parts of inner shelf facies) and lower parts of
282 allochthons. Similar intrabasement, high amplitude and dipping reflections are interpreted as orogenic
283 and postorogenic shear zones in the Norwegian Caledonides (Phillips et al., 2016; Fazlikhani et al.,
284 2017; Wrona et al., 2020; Osagiede et al., 2019), offshore Brazil (Strugale et al., 2021; Vasconcelos et
285 al., 2019), offshore New Zealand (Collanega et al., 2019; Phillips and McCaffrey, 2019), and in the
286 South China Sea (Ye et al., 2020). High amplitude and continuous reflections of BSF2 below the
287 Münchberg nappe and across the FFS to the west are therefore interpreted as the W-SW extension of
288 a Variscan detachment/shear zone transporting allochthonous nappes and underlying
289 metasedimentary rocks W-SW, towards the Franconian Basin area. BSF2 reflections generally get
290 shallower from east to west and reach the base of the overlying sedimentary units.

291 **3.4.3 Basement Seismic Facies 3 (BSF3)**

292 Basement Seismic Facies 3 (BSF3) is characterized by semi-continuous and medium-amplitude
293 reflections (Fig. 4A & D). BSF3 is bounded by BSF2 at the top and extends to the lower limit of the
294 dataset at 8 s TWT. BSF3 does not show any preferential dip direction and locally hosts some higher
295 amplitude, continuous and dipping reflections of BSF2. Such high amplitude reflections of BSF2 are
296 branching off the main BSF2 packages or are developed at deeper levels and are interpreted as
297 segments of major shear zones or locally developed shear zones of Variscan origin. BSF3 is not drilled
298 by wells, nevertheless considering the tectonostratigraphic position of BSF3 below the Variscan
299 detachment/shear zones (BSF2), BSF3 is interpreted to represent Cadomian basement rocks and
300 overlaying Paleozoic Inner shelf facies not involved in Variscan tectonics.

301 **4 Seismic reflection Interpretation of the FRANKEN seismic survey**

302 Described seismic facies in the sedimentary cover and underlying basement units and well information
303 are utilized in this chapter to interpret the FRANKEN seismic profiles.

304 **4.1 Profile FRANKEN-1801**

305 Profile FRANKEN-1801 is 47.9 km long and extends NW-SE from south of Bamberg to the NW of
306 Haßfurt (Fig. 1). At the surface, mainly Keuper units are exposed (Fig. 1). Thicknesses of remnant
307 Keuper units progressively decrease to the W-NW and at the northwestern edge of profile FRANKEN-
308 1801, Muschelkalk units are exposed at the surface in the footwall of a segment of the Kissingen-
309 Haßfurt Fault Zone (Fig. 6). This fault zone is mapped over ca. 60 km with ca. 7-10 km width, sub-
310 parallel to the NW-SE striking FRANKEN-1801 profile (Fig. 1). Some segments of the Kissingen-Haßfurt
311 Fault Zone are oblique and are imaged by the FRANKEN-1801 profile. Muschelkalk and Buntsandstein
312 units are fairly tabular with no major lateral thickness changes (Fig. 6). Most of the interpreted faults
313 (seismic scale) are normal faults, while major reverse faults are sub-parallel to the profile and are not
314 imaged in FRANKEN-1801.

315 Below the Buntsandstein, Permian deposits including 114 m Zechstein and 3 m Rotliegend have been
316 drilled by well Eltmann, 2230 m to the NE of profile FRANKEN-1801 (Fig. 6) (Trusheim, 1964). Semi-
317 continuous and medium-amplitude reflections below the Zechstein are interpreted as Rotliegend
318 deposits (Fig. 6). As the Rotliegend base is not particularly reflective in the seismic reflection data, it is

319 difficult to interpret the top basement. Towards the NW in the center of the FRANKEN-1801 profile,
320 BSF1 reflections (Paleozoic metasedimentary rocks and Variscan nappes) are present below the
321 Permian rocks and are underlain by a Variscan shear zone (BSF2, Fig. 6). From the SE, the Variscan
322 shear zone shallows to the NW and reaches ca. 700 ms TWT at the center of the profile (Fig. 6).

323 **4.2 Profile FRANKEN-1802**

324 Profile FRANKEN-1802 extends NE-SW with 47.7 km length (Fig. 1). This profile is at a high angle to the
325 prominent NW-SE faults, and therefore provides a good subsurface image of these structures (Fig. 7).
326 Profile FRANKEN-1802 is tied to the well Eltmann and runs close to wells Mürsbach 6 (630 m to the S),
327 Staffelstein 1 (1235 m, to the SE) and Staffelstein 2 (890 m, to the SE). Profile FRANKEN-1802 is used
328 as the reference profile for the seismo-stratigraphic interpretation (Fig. 7). Jurassic rocks are preserved
329 in the footwall of the Mürsbach and Lichtenfels reverse faults drilled with 104 m thickness by well
330 Staffelstein 2 (Table 1; (Gudden, 1977). Keuper strata are exposed in the hanging wall of the
331 Lichtenfels Fault at the northeastern edge of profile FRANKEN-1802 (Fig. 7). Keuper is drilled with 532
332 m in thickness by well Staffelstein 2. Towards the SW the Keuper is increasingly eroded and only 178.6
333 m are preserved at the location of well Eltmann (Fig. 7 and Table 1, (Gudden, 1977; Trusheim, 1964).
334 Muschelkalk and Buntsandstein sedimentary rocks are tabular and regionally dip to the E-NE (Fig. 7).
335 The Zechstein is penetrated by wells Eltmann, Mürsbach 1 and 6, and Staffelstein 1 and is 103-121 m
336 thick (Table 1; (Gudden, 1985). Below the Zechstein units, Rotliegend is drilled by wells Eltmann,
337 Mürsbach 1 and 6 and Staffelstein 1 without reaching the underlying basement, except in well Eltmann
338 (Table 1). Medium-amplitude and semi-continuous reflections, characteristic of the Rotliegend in the
339 study area, are also locally observed, suggesting the presence of Rotliegend laterally away from wells
340 (Fig. 7). Rotliegend units are wedge shape and are tilted to the E-NE, onlapping to deep sited W-SW
341 dipping normal faults in the footwall of the Mürsbach and Lichtenfels reverse faults (Fig. 7).
342 Interpreted W-SW dipping normal faults appear to be crosscut by the oppositely dipping (E-NE)
343 Lichtenfels and Mürsbach reverse faults in Buntsandstein units (Fig. 7). E-NE block rotation in the
344 hangingwall of these normal faults created local half-grabens observed exclusively in the Rotliegend
345 section (Fig. 7). In the hanging wall of a normal fault located in the footwall of Lichtenfels Fault, the
346 thickness of the Permian section is > 330 ms TWT (ca. 640 m) thinning W-SW to ca. 120 ms TWT (ca.
347 240 m) in the hangingwall of the Mürsbach Fault (Fig. 7). The interpretation of lateral thickness
348 changes in the Permian is in good accordance with 142.3 m minimum thickness of Permian drilled in
349 well Mürsbach 6 (Table 1). The thickness of the Permian section in the hanging wall of Bamberg Fault
350 is > 200 ms TWT (ca. 390 m) decreasing to the W-SW down to 3 m, drilled by well Eltmann (Fig. 7).

351 Sedimentary units in the hanging wall of the Lichtenfels Fault are uplifted and gently folded where the
352 entire Jurassic and the upper parts of the Upper Triassic Keuper Group are eroded (Fig. 7). In the
353 footwall of the Lichtenfels Fault sedimentary units are folded by a normal drag fold, creating a local
354 synform structure (also known as Hollfeld Syncline) where Jurassic rocks are preserved (Fig. 7). The
355 NW-SE striking Lichtenfels Fault is laterally and vertically segmented and is exposed at the surface over
356 ca. 16 km length (Fig. 1). In profile FRANKEN-1802, the Lichtenfels Fault has 135 ms TWT (ca. 260 m)
357 throw, measured at the top of the Buntsandstein (Fig. 7). The Mürsbach Fault strikes NNW-SSE over
358 ca. 5 km and it has been imaged by the Mürsbach seismic survey along three short (<4 km) 2D seismic
359 sections (Unpublished internal report, Flemm, H., Körner, H.-J., Dostmann, H., and Lemcke, k. 1971).
360 The Mürsbach Fault shows ca. 65 ms TWT (ca. 120 m) throw measured at the Buntsandstein top. Both,
361 Muschelkalk and Keuper units are folded, creating a local anticline in the hangingwall of the Mürsbach
362 Fault. Upper parts of the Keuper and younger units are eroded on the hangingwall side while in the
363 immediate footwall some of the Jurassic units are still preserved (Fig. 7). E-NE dipping normal faults

364 interpreted in the SW part of the profile FRANKEN-1802 are subparallel to the SE extension of the
365 Kissingen-Haßfurt Fault Zone (Fig. 7).

366 In the well Eltmann 94 m of ?Devonian metasedimentary rocks are drilled below the sedimentary
367 cover and correlated with BSF1 (Fig. 7; Trusheim, 1964). Identified BSF1 units are ca. 800 ms TWT (ca.
368 1560 m) thick in the NE of the seismic section, decreasing to 94 m towards the SW at the location of
369 well Eltmann. BSF2 reflections show a concave up geometry below the Lichtenfels and Mürsbach faults
370 and extend to shallower depth towards the west (Fig. 7). In the center of the profile some high
371 amplitude reflections of BSF2 branch off from the main reflection package and extend into the deeper
372 parts of the crust (Fig. 7).

373 **4.3 Profile FRANKEN-1803**

374 This profile is subparallel to the profile FRANKEN-1801 and strikes NW-SE over 71.8 km length (Fig. 1).
375 Well Obernsees is located 945 m SW of this profile and drilled into 140 m of Jurassic, the entire Triassic
376 succession and 104.9 m of upper Permian Zechstein units (Table 1 and Fig. 8, (Helmkamp, 2006).
377 Jurassic units are preserved at the surface, except in the SE and NW parts of profile 1803, indicating a
378 gentle synformal geometry with remnant Jurassic units thickest in the center of the profile (Fig. 8).
379 Triassic intervals show subparallel boundaries with only minor lateral thickness changes. At well
380 Obernsees, the Rotliegend is only 18.3 m thick overlying metasedimentary rocks of possible late
381 Paleozoic age (Stettner and Salger, 1985; Ravidà et al., 2021). The reduced thickness of Rotliegend
382 units in well Obernsees is related to a local basement high in the footwall of an ESE-dipping normal
383 fault (Fig. 8). In the hanging wall of this normal fault and to the SE, medium amplitude and semi-
384 continuous reflections below the top Zechstein horizon are interpreted as Rotliegend (Fig. 8, (Stettner
385 and Salger, 1985; Schuh, 1985). Permian units are underlain by Paleozoic metasedimentary rocks and
386 Variscan nappes (BSF1 units, Fig. 8). BSF2 reflections are sub-horizontal (between 2000-2500 ms, TWT)
387 and gradually get shallower to the NW to reach to ca. 1200 ms TWT. From the SE to the center of the
388 profile, BSF2 reflections become less pronounced and appear to be segmented, into a steeper and a
389 sub-horizontal segment (Fig. 8). Farther NW, BSF2 reflections reach to shallower depth and are also
390 imaged by the perpendicular FRANKEN-1802 and 1804 profiles. Lateral segmentation and changes in
391 the reflectivity of the BSF2 might be related to the 3D geometry of an interpreted detachment/shear
392 zone (Fig. 8).

393 **4.4 Profile FRANKEN-1804**

394 This profile strikes NE-SW over 63.3 km length, subparallel to the profile FRANKEN-1802 (Fig. 9).
395 Jurassic units are preserved in the NE and the central part of the profile. To the SW however, Jurassic
396 units are eroded and Keuper sandstones are exposed at the surface (Fig. 9). Geometries of Triassic
397 units are fairly tabular, generally with shallow dips to the NE-E, but with variable dip angles between
398 fault blocks. High amplitude and continuous reflections below the Triassic units are interpreted as
399 Zechstein and are correlated with similar reflection packages in perpendicular profiles FRANKEN-1801
400 and 1803. Semi-continuous and medium amplitude reflections beneath the Zechstein are interpreted
401 as Rotliegend that locally onlaps to the hanging wall of deep-seated W to SW dipping normal faults
402 (Fig. 9). In general, Permian units are wedge shaped in the hanging walls of normal faults and thin
403 laterally. Paleozoic metasedimentary units and Variscan nappes (BSF1) underlie the Permian and are
404 ca. 1400 ms TWT (ca. 2700 m) thick in the center of the profile but thin laterally. Variscan shear zone
405 (BSF2) underlying Paleozoic metasedimentary units and Variscan nappes are concave-shaped in the
406 NE and reach to shallower depth towards the southwestern edge of the profile FRANKEN-1804 (Fig.
407 9). In the center of the profile, BSF2 reflections are observed at greater depth up to about 3000 ms

408 TWT and are slightly less reflective. Cadomian basement and parts of inner shelf facies not involved in
409 Variscan tectonics (BSF3) characterize the deeper parts of the profile FRANKEN-1804 (Fig. 9).

410 At the NE edge of the profile FRANKEN-1804, the Eisfeld-Kulmbach Fault accumulates ca. 660 ms TWT
411 (ca. 1280 m) of throw, exposing Buntsandstein in its hangingwall (Fig. 9). Across the fault, Jurassic units
412 are preserved in the footwall and thin towards the SW where they are eroded in the hangingwall of
413 the Asslitz Fault (Fig. 9). The Asslitz Fault accumulates ca. 210 ms TWT (ca. 420 m) of throw at the top
414 of the Buntsandstein. Farther SW, the Lichtenfels Fault offsets Permian to Upper Triassic units with
415 ca. 90 ms TWT (ca. 170 m) of throw measured at the Muschelkalk top. In contrast to profile FRANKEN-
416 1802 (ca. 9 km NW), along the profile FRANKEN-1804 Lichtenfels Fault does not reach to the surface
417 and dies out within the Keuper units. In the footwall of Lichtenfels Fault a W toSW dipping normal
418 fault creates a local half-graben where continuous and medium amplitude reflections are onlapping
419 and terminating against the fault (Fig. 9). Further SW, Bamberg Fault is a major normal fault displacing
420 the Triassic and Permian units with ca. 40 ms TWT (ca. 80 m) offset measured at top Muschelkalk.
421 Bamberg Fault detaches into the underlying Variscan shear zone (BSF2) at depth (Fig. 9). Farther north
422 along the profile FRANKEN-1802, Bamberg fault is displaced by the Mürsbach reverse fault (Fig. 7).

423 **5 Discussion**

424 **5.1 Westward extension of the Saxothuringian zone**

425 Exposed Variscan allochthons are tectonically placed above the Paleozoic outer shelf facies (Bavarian
426 facies) defined as fine grained and clay rich material preserved around and below Variscan nappe piles
427 (Linnemann and Heuse, 2001; Franke and Stein, 2000). BSF1 units observed beneath the sedimentary
428 cover west of the FFS (Figs. 7 and 9) are interpreted as equivalents of Paleozoic metasedimentary
429 rocks and Variscan nappe units (e.g. Münchberg nappe, Fig. 10). BSF1 units are mapped as far as ca.
430 65 km west of the FFS and are thinning towards the NW along the NW-SE striking profiles (Figs. 6 and
431 8) and towards the SW along the NE-SW striking profiles (Figs. 7 and 9), showing a general westward
432 thinning of Variscan nappes and Paleozoic metasedimentary rocks. Wells drilled in the Schwarzwald
433 and Upper Rhein Graben areas (ca. 300 km SW of the study area) show low-grade metasedimentary
434 units (shales and phyllites) and volcanic rocks below sedimentary cover, interpreted as SW extension
435 of the Saxothuringian Zone (Franke et al., 2017). Although seismic reflection and few well data confirm
436 the presence of low- to very low-grade metasedimentary rocks below the Permian to Jurassic
437 sedimentary cover in the study area, no well has probed the Variscan nappes west of the FFS yet.
438 Seismic signatures of exposed Variscan nappes and low grade metasedimentary rocks east of the FFS
439 do not allow differentiation between nappes and metasedimentary rocks. Similar observations have
440 been made in the Caledonides of western Norway (Fazlikhani et al., 2017; Lenhart et al., 2019).
441 Differentiation of Paleozoic inner and outer shelf facies is also beyond the resolution of available
442 seismic reflection data. However, the tectonostratigraphic position of Variscan nappes and
443 metasedimentary rocks relative to basal shear zones in exposed basement units east of the FFS (Heuse
444 et al., 2010; Linnemann et al., 2010), supports the possible presence of Variscan nappes and
445 underlying inner and outer shelf facies ca. 65 km west of FFS (Fig. 10).

446 In the exposed parts of the Saxothuringian zone east of FFS, kinematic indicators show a top-to-the
447 W-SW tectonic transport under NE-SW compression (Schwan, 1974). This deformation phase has been
448 described as "D1" deformation phase and is related to the subduction and collision during the Variscan
449 Orogeny before ca. 340 Ma (Kroner et al., 2007). For the assemblage of the Variscan during the
450 subduction and collision, a top-to-the NW tectonic transport under a NW-SE compression has also
451 been proposed (Franke and Stein, 2000). Observed regional westward shallowing of mapped thrust
452 shear zones west of FFS could have been developed under both proposed tectonic transport
453 directions. Seismic reflection data does not allow to define a preferred tectonic transport direction,
454 however, based on the kinematic indicators observed and described in the exposed parts of the
455 Saxothuringian Zone, we tend to prefer the W-SW transport direction.

456 **5.2 Shear zone topography and strain localization during brittle deformation**

457 A regional NW-SE dominated compressional and dextral transpressional phase at ca. 340-330 Ma
458 affected the Saxothuringian zone and most likely reactivated preexisting D1 shear zones including the
459 Münchberg Shear Zone, MSZ (Franke, 2000; Kroner et al., 2007). The 340-330 Ma dextral transpression
460 in addition to NE-SW regional compression during the D1 deformation phase might be responsible for
461 modifying the initial geometry of the mapped shear zone by folding and bending (Figs. 7 and 9). Latest
462 to post orogenic normal faults appear to be developed in wide range of vertical and lateral scale in
463 response to the regional stress field. These normal faults propagate radially and create larger faults
464 (e.g. Fazlikhani et al., 2021). However, only the ones that detach into the shear zone or preexisting
465 thrust faults at depth further grow and potentially reactivate parts of the shear zone on their
466 hangingwall side, while other normal faults become inactive (Figs. 7, 9 and 11b).

467 All the major reverse faults (Eisfeld-Kulmbach, Asslitz, Lichtenfels (northern portion) and Mürsbach
468 faults) most likely developed in response to Cretaceous inversion event in central Europe (Kley and
469 Voigt, 2008) concentrate around the antiformal parts of the shear zone. For example, along the
470 FRANKEN-1802 profile, the Lichtenfels Fault developed on top of the folded portion of the underlying
471 shear zone and it is exposed at the surface (Fig. 7). Whereas ca. 10 km farther south along the
472 FRANKEN-1804 profile where the underlying shear zone show a rather flat geometry, the Lichtenfels
473 Fault does not reach to the surface (Fig. 9). Similarly, the Mürsbach reverse fault in the footwall of the
474 Bamberg normal fault (or a similar normal fault) developed on top of the folded portion of the shear
475 zones and dies out laterally to the south where the shear zone is rather flat (Fig. 7 and 9). Our
476 observations demonstrate that antiformal geometry of shear zone seems to perturb the regional
477 stress field and localize the strain around the antiformal portions of the shear zone facilitating lateral
478 and vertical growth of preferentially located brittle faults (Fig. 12). Comparable strain localization and
479 brittle reactivation of orogenic shear zones during initiation and activity of post-orogenic brittle faults
480 has been described from the post-Caledonian tectonics in Scandinavia (Fazlikhani et al., 2017; Phillips
481 et al., 2016; Koehl et al., 2018; Wiest et al., 2020) and post-Variscan tectonics of the western Alps
482 (Festa et al., 2020; Ballèvre et al., 2018). Geometry of shear zone creating local ramp also appears to
483 influence the magnitude of fault offset in the study area. In the northeastern part of FRANKEN-1802
484 profile where the Variscan shear zone shows antiformal geometry, the Lichtenfels Fault accumulates
485 ca. 180 ms TWT of throw at the top Muschelkalk horizon and it is exposed at the surface. Along the
486 FRANKEN-1804 profile, ca. 10 km farther south, where the Variscan shear zone shows a rather flat
487 geometry, the Lichtenfels Fault has only ca. 90 ms TWT of throw and is a blind fault tipping out in the
488 Keuper units. In addition, at the location of antiformal parts of the shear zone generally a higher
489 amount of upper crustal brittle deformation (normal and reverse faults) occurs (Figs. 7 and 9). It should
490 be noted that towards the east, at the margin of the Franconian Basin, the FFS as the major basin
491 bounding fault system displaces the basal detachment/shear zone, exposing Variscan basement units
492 in the hangingwall side. Comparing reverse faults with few hundred meters of offset detaching into
493 the shear zones with the FFS having ca. 3 km of offset (Wagner et al., 1997) displacing the shear zone,
494 shows that large amount of accumulative fault offset can breakthrough and displace the underlying
495 shear zone. The amount of fault offset together with the previously shown mechanical/rheological
496 properties of shear zones and their orientation relative to the extension/shortening direction are thus
497 important controlling factors in reactivation or displacement of the basal detachment/shear zone by
498 brittle faults (Daly et al., 1989; Ring, 1994; Peace et al., 2018; Heilman et al., 2019; Phillips et al., 2019).

499 **5.3 Post Variscan Rotliegend basins in SE Germany and their regional context**

500 The latest stages of Variscan tectonics and post orogenic thermal relaxation during the late
501 Carboniferous and early Permian are marked by the development of intermontane basins in the

502 internal parts of the Variscan belt (Arthaud and Matte, 1977; McCann et al., 2006). These
503 intermontane basins are mainly located in the hangingwall of normal faults in graben and half-graben
504 settings and therefore are relatively small (km to tens of km), deep and isolated basins accumulating
505 continental clastic sediments with rapid lateral thickness changes (McCann et al., 2006). Fault-
506 bounded Rotliegend basins in SE Germany are also interpreted to have developed in an extensional
507 and/or transtensional setting during latest Carboniferous and Permian times as evidenced by rather
508 abrupt lateral thickness and sedimentary facies changes across normal faults (Schröder, 1988, 1987;
509 Peterek et al., 1996c; Leitz and Schröder, 1985; Arthaud and Matte, 1977; Dill, 1988; Müller, 1994;
510 Peterek et al., 1997; McCann et al., 2006; Helmkamp et al., 1982). Rotliegend sedimentary rocks in
511 the study area are exposed in the footwall and hangingwall of the FFS from NW to SE in the Stockheim,
512 Rugendorf, Wirsberg and Weidenberg outcrops (Fig. 1). Well Wolfersdorf (Stockheim outcrop) drilled
513 726 m of Rotliegend, while the upper parts of the section are eroded, suggesting that originally even
514 thicker Rotliegend sections (ca. 1000 m) were deposited (Herrmann, 1958; Dill, 1988; Paul and
515 Schröder, 2012). About 18 km west of well Wolfersdorf, well Mittelberg drilled only 41 m of Rotliegend
516 before reaching basement rocks (Friedlein and Hahn, 2018). Similar rapid thickness changes of the
517 Rotliegend units were also observed in the Weidenberg, Erbdorf, Weiden and Schmidgaden areas,
518 all originally interpreted as small, isolated fault-bounded basins, but now, interpreted as individual
519 exposures of one coherent depositional area, the NW-SE Naab Basin, where the Rotliegend reaches
520 up to 2800 m thickness (Paul and Schröder, 2012). The Naab Basin is bordered by normal faults, some
521 of which were reactivated as reverse faults or cross cut by younger reverse faults (Müller, 1994;
522 Peterek et al., 1996b).

523 In addition to exposures along the FFS, several wells in the western parts of the study area (e.g.
524 Staffelstein 1, Mürsbach 1 & 6, and Eltmann) also encountered Rotliegend that relates to the SW-NE
525 Kraichgau Basin (Table 1, Fig. 1) of which the NW-SE Naab Basin is considered a basin compartment
526 (Paul, 2006). Among these wells, only Eltmann and Mittelberg reached the Rotliegend base showing a
527 general westward thinning of Rotliegend units from the FFS (Table 1). This corresponds to the pattern
528 of isopach maps, showing a gradual thickening of Rotliegend units to reach maximum thicknesses of
529 ca. 2000 m in the easternmost parts of the Kraichgau Basin (Sitting and Nitsch, 2012).

530 Rotliegend basin architecture in the Variscan Internides, with the Saar-Nahe, Kraichgau and
531 Schramberg basins as prominent examples, is characterized by 10-100 km wide and long basins
532 bordered by normal faults, rather related to extensional forces than the collapse of overthickened
533 crust during the orogeny (Henk, 1997). In comparison, post-Caledonian Devonian basins in western
534 Norway developed as supra-detachment basins that are bounded by brittle normal faults reactivating
535 pre-existing Caledonian thrusts (Fossen, 2010; Fazlikhani et al., 2017; Wiest et al., 2020; Lenhart et al.,
536 2019; Séranne and Séguret, 1987; Osmundsen and Andersen, 2001). Post-Caledonian
537 supradetachment basins in western Norway accumulate >26 km thick of Devonian units that is almost
538 three times more than the true depth of the basin (Vetti and Fossen, 2012; Séranne and Séguret,
539 1987). In the northern North Sea and its western margin onshore Scotland and Shetland, and offshore
540 East Shetland Platform, post-Caledonian Devonian basins are interpreted as normal fault bounded
541 half-graben basins that in some cases detach onto Caledonian thrust/shear zones (Coward et al., 1989;
542 Platt and Cartwright, 1998; Fazlikhani et al., 2017; Norton et al., 1987; Séranne, 1992; Patruno et al.,
543 2019; Phillips et al., 2019; Fazlikhani et al., 2021).

544 The range of post-orogenic basin architecture observed in Caledonian and Variscan orogens highlights
545 the importance of preexisting orogenic thrust/shear zones. Comparison of post-Caledonian basins
546 with post-Variscan basins shows that in the Caledonian cases pre-existing detachment/shear zone play
547 a more important role in basin development and architecture than in the post-Variscan basins, as

548 observed in the study area. Normal faults bounding post-Variscan basins appear not to reactivate
549 entire Variscan thrust/shear zones except for the Saar-Nahe Basin (Henk, 1993). Observed variations
550 in post-orogenic basin architecture might be related to the differences in the exposed level of the
551 basement. Exposed Devonian basins of western Norway show deeper levels of crust in comparison to
552 Devonian basins in the western margin of the North Sea rift. It should be noted that the post-orogenic
553 extension direction relative to the orientation of the orogenic structures in addition to the amount
554 and duration of the post-orogenic extension also influence basin architecture.

555

556 **5.4 Brittle fault development and relative age relationships**

557 Post-Variscan extensional phases resulted in the development of normal faults bounding Rotliegend
558 half-graben and graben basins observed across the Variscan belt (Peterek et al., 1997; Arthaud and
559 Matte, 1977; McCann et al., 2006; Schröder, 1987; Müller, 1994; Stephenson et al., 2003). Mapped
560 seismic scale normal faults in the study area can be divided into three main groups, based on their
561 stratigraphic position: I) normal faults developed at shallower depth which terminate in the Lower
562 Triassic or upper Permian (Zechstein) intervals (Figs. 6-9). II) normal faults developed in the deeper
563 parts of the stratigraphy displacing Permian units and continuing into the pre-Permian units with their
564 upper tip terminating in uppermost Permian (Zechstein) or lowermost Triassic units (e.g. normal faults
565 in the footwall of Lichtenfels and Asslitz reverse faults, Figs. 6-9). III) small groups of normal faults
566 which displace the entire stratigraphy and die out into the pre-Permian units (Figs. 6 and 9).

567 The first group of normal faults which developed in the Triassic units only, do not show
568 synsedimentary activity detectable in seismic profiles and are interpreted to most likely originate from
569 sedimentary loading and differential compaction during a regional tectonic quiescence in Triassic and
570 Jurassic times (Peterek et al., 1997; Fazlikhani et al., 2021; Fazlikhani and Back, 2015). The second
571 group of normal faults, displacing mainly the Permian succession, is interpreted to have developed
572 during post-orogenic extension in latest Carboniferous-Permian (Stephanian/Rotliegend) time. This
573 second group of normal faults shows widespread evidence of synsedimentary activity and bounding
574 Permian half graben and graben basins (buried and exposed) in southern Germany. In the majority of
575 cases the first and second groups of normal faults are not vertically hard-linked. This observation can
576 be explained by the presence of fine grained marine and in some places evaporitic Zechstein units,
577 acting as a semi-ductile to ductile layer accommodating strain. However, in few instances the
578 Zechstein, together with Triassic units is displaced by the third group of normal faults (Figs 6 and 9). It
579 should be noted that with the available dataset it is not clear whether the third group of normal faults
580 is the result of an upsection growth of Permian faults, downsection growth of the Triassic-Jurassic
581 faults or whether they developed due to the downsection growth of Triassic –Jurassic faults linking to
582 and reactivating preexisting Permian faults.

583 In addition to normal faults, the major km-long NW-SE striking Eisfeld-Kulmbach, Asslitz, Lichtenfels
584 and Mürsbach reverse faults are located west of the FFS, displacing and folding the Permian to Jurassic
585 sedimentary cover. Reverse faults are better developed in the eastern part of the study area and on
586 top of the antiformal parts of the Variscan shear zones while towards the west, normal faults
587 dominate. Observed reverse faults are developed mainly in the footwalls of Permian normal faults and
588 dip to the E-NE (Figs. 6-9). Reverse faults cut through the upper portion of Permian normal faults,
589 translating Permo-Mesozoic units to the W-SW. Farther north of the study area in the Thuringian Basin
590 and northern Germany, similar reverse faults are related to the Cretaceous inversion event (Kley and
591 Voigt, 2008; Navabpour et al., 2017). Therefore, it appears that the youngest generation of seismic-
592 scale brittle faults are the reverse faults. However, whether reverse faults only initiated during the
593 Cretaceous inversion and younger events or rather are reverse reactivated east dipping Permian
594 normal faults is still unclear and needs further investigation.

595 6 Conclusion

596 In this study we combine existing 2D seismic reflection profiles, well data and surface geological
597 information to interpret the recently acquired 2D FRANKEN seismic survey in SE Germany. Three
598 Basement Seismic Facies (BSF1-3) are described below the Permian-Mesozoic sedimentary cover that
599 are interpreted as Variscan units and structures. We investigate the possible westward continuation
600 of Variscan units and structures and discuss the influence of Variscan structures in latest to post-
601 Variscan basin development. We show that:

- 602 • Variscan units and structures extend to ~65 km west of the FFS beneath sedimentary rocks of
603 the Kraichgau/Franconian Basin.
- 604 • Low-grade metasedimentary rocks and possible nappe units (BSF1) in the hanging wall of
605 Variscan shear zones are wedge shaped and thin out towards the W-SW.
- 606 • Variscan autochthons occupy the footwalls of shear zones.
- 607 • Shear zones show local syn- and antiformal geometries and reach to the base of the Permian-
608 Mesozoic sedimentary cover towards the W-SW.
- 609 • The geometry of shear zones control the location at which major Permian normal faults have
610 developed.
- 611 • Permian normal faults dip in various directions, creating Rotliegend graben and half-graben
612 basins. Observed Rotliegend half-graben basins in the east are interpreted as the NW
613 continuation of the Naab Basin. Towards the west, interpreted Rotliegend units are associated
614 to the Kraichgau Basin.
- 615 • The thickness of Triassic sedimentary rocks is fairly constant, highlighting a regional tectonic
616 quiescence in the study area.
- 617 • Some of the Permian normal faults are cross cut by oppositely dipping reverse faults most
618 likely during the regional Cretaceous inversion event that occurred in Central Europe. Some
619 of reverse faults are interpreted as reactivated preexisting Permian normal faults, while others
620 might have been developed during the Cretaceous inversion event.
- 621 • Reverse reactivated normal faults are restricted to the eastern parts of the study area where
622 preexisting Variscan shear zone show syn- and antiformal geometries.

623 We document westward continuation of Variscan shear zones away from the Bohemian Massif for the
624 first time and show how the geometry of shear zones localize the strain and influence the
625 development of latest to post-orogenic faults and basins.

626

627 Data availability

628 DEKORP seismic data are available via GFZ (Deutsche GeoForschungsZentrum) Potsdam. Utilized well
629 data can be accessed through the Geological Survey of Bavaria (Bayerisches Landesamt für Umwelt -
630 LfU). FRANKEN seismic data are acquired for the ongoing Geothermal Alliance Bavaria (GAB) research
631 project and are not publically available yet.

632

633 Author contributions

634 Hamed Fazlikhani integrated utilized datasets, interpreted seismic reflection and prepared the
635 manuscript. Wolfgang Bauer planned and managed the seismic data acquisition and with Harald

636 Stollhofen acquired the financial support and contributed to the reviewing, improvement and the
637 discussion of the presented results.

638

639 **Competing interests**

640 The authors declare that they have no conflict of interest.

641

642 **Acknowledgment**

643 This contribution is part of the Geothermal Alliance Bavaria (GAB) project funded by the Bavarian State
644 Ministry of Education and Cultural Affairs, Science and Art to the Friedrich-Alexander-University
645 Erlangen-Nuremberg (FAU), The Technical University of Munich (TUM) and the University of Bayreuth.
646 We would like to thank the Bayerisches Landesamt für Umwelt (LfU) for providing well data and fruitful
647 discussions. Schlumberger is thanked for providing academic licenses for Petrel and supporting the
648 “3D Lab” at the Friedrich-Alexander-University Erlangen-Nuremberg. Authors would like to thank
649 members of the GAB project for the discussions increasing the quality of this contribution. Topical
650 editor Virginia Toy, reviewers Jonas Kley, Uwe Kroner and anonymous referee and community
651 comment of Jean-Baptiste Koehl are thanked for their comments which greatly improved the quality
652 of our manuscript.

653

654 **References**

- 655 Arthaud, F. and Matte, P.: Late Paleozoic strike-slip faulting in southern Europe and northern Africa:
656 Result of a right-lateral shear zone between the Appalachians and the Urals, *GSA Bulletin*, 88,
657 1305–1320, [https://doi.org/10.1130/0016-7606\(1977\)88<1305:LPSFIS>2.0.CO;2](https://doi.org/10.1130/0016-7606(1977)88<1305:LPSFIS>2.0.CO;2), 1977.
- 658 Bader, K. and Bram, K. (Eds.): *Der mittelfränkische Gebirgsrücken südlich Nürnberg*, Schweizerbart
659 Science Publishers, Stuttgart, Germany, 2001.
- 660 Ballèvre, M., Manzotti, P., and Dal Piaz, G. V.: Pre-Alpine (Variscan) Inheritance: A Key for the
661 Location of the Future Valaisan Basin (Western Alps), *Tectonics*, 37, 786–817,
662 <https://doi.org/10.1002/2017TC004633>, 2018.
- 663 Behr, H. J. and Heinrichs, T.: Geological interpretation of DEKORP 2-S: A deep seismic reflection
664 profile across the Saxothuringian and possible implications for the Late Variscan structural
665 evolution of Central Europe, *Tectonophysics*, 142, 173–202, [https://doi.org/10.1016/0040-](https://doi.org/10.1016/0040-1951(87)90122-3)
666 [1951\(87\)90122-3](https://doi.org/10.1016/0040-1951(87)90122-3), available at:
667 <https://www.sciencedirect.com/science/article/pii/0040195187901223>, 1987.
- 668 Bergerat, F. and Geysant, J.: Tectonique cassante et champ de contraintes tertiaire en avant des
669 Alpes orientales: le Jura souabe, *Geologische Rundschau*, 71, 537–548, 1982.
- 670 Boy, J. A., Haneke, J., Kowalczyk, G., Lorenz, V., Schindler, T., Stollhofen, H., and Thum, H.: Rotliegend
671 im Saar-Nahe-Becken, am Taunus-Südrand und im nördlichen Oberrheingraben, in:
672 *Innervariscische Becken*, edited by: Lützner, H., Schweizerbart Science Publishers, Stuttgart,
673 Germany, 254–377, 2012.
- 674 Buness, H.-A. and Bram, K.: Die Muschelkalkoberfläche und die permische Peneplam in
675 Mittelfranken abgeleitet aus seismischen Messungen, in: *Der mittelfränkische Gebirgsrücken*
676 *südlich Nürnberg*, edited by: Bader, K. and Bram, K., Schweizerbart Science Publishers, Stuttgart,
677 Germany, 35–59, 2001.
- 678 Carlé, W.: *Bau und Entwicklung der Südwestdeutschen Großscholle*, Beihefte zum Geologischen
679 *Jahrbuch*, 1955.

680 Cassinis, G., Toutin-Morin, N., and Virgili, C.: A General Outline of the Permian Continental Basins in
681 Southwestern Europe, in: *The Permian of Northern Pangea.: Volume 2: Sedimentary Basins and*
682 *Economic Resources*, edited by: Scholle, P., Peryt, t. M., and Ulmer-Scholle, D. S., Springer, Berlin,
683 137–157, 1995.

684 Chateauneuf, J. J. and Farjanel, G.: *Synthèse Géologique des Bassins Permians Français*, 128th ed.,
685 1989.

686 Collanega, L., Siuda, K., A.-L. Jackson, C., Bell, R. E., Coleman, A. J., Lenhart, A., Magee, C., and Breda,
687 A.: Normal fault growth influenced by basement fabrics: The importance of preferential
688 nucleation from pre-existing structures, *Basin Res*, 31, 659–687,
689 <https://doi.org/10.1111/bre.12327>, 2019.

690 Coubal, M., Málek, J., Adamovič, J., and Štěpančíková, P.: Late Cretaceous and Cenozoic dynamics of
691 the Bohemian Massif inferred from the paleostress history of the Lusatian Fault Belt, *Journal of*
692 *Geodynamics*, 87, 26–49, <https://doi.org/10.1016/j.jog.2015.02.006>, 2015.

693 Coward, M. P., Enfield, M. A., and Fischer, M. W.: Devonian basins of Northern Scotland: extension
694 and inversion related to Late Caledonian — Variscan tectonics, Geological Society, London,
695 *Special Publications*, 44, 275, <https://doi.org/10.1144/GSL.SP.1989.044.01.16>, 1989.

696 Daly, M. C., Chorowicz, J., and Fairhead, J. D.: Rift basin evolution in Africa: the influence of
697 reactivated steep basement shear zones, Geological Society, London, *Special Publications*, 44,
698 309–334, <https://doi.org/10.1144/GSL.SP.1989.044.01.17>, 1989.

699 DEKORP and Orogenic Processes Working Group: Structure of the Saxonian Granulites: Geological
700 and geophysical constraints on the exhumation of high-pressure/high-temperature rocks in the
701 mid-European Variscan belt, *Tectonics*, 18, 756–773, <https://doi.org/10.1029/1999TC900030>,
702 1999.

703 DEKORP Research Group: Crustal structure of the Saxothuringian Zone: Results of the deep seismic
704 profile MVE-90(East), *Zeitschrift für Geologische Wissenschaften*, 22, 647–769, available at:
705 <http://www.zgw-online.de/en/>, 1994a.

706 DEKORP Research Group: DEKORP 3/MVE 90(West) - preliminary geological interpretation of a deep
707 near-vertical reflection profile between the Rhenish and Bohemian Massifs, Germany, *Zeitschrift*
708 *für Geologische Wissenschaften*, 22, 771–801, 1994b.

709 Dill, H.: *Sedimentpetrographie des Stockheimer Rotliegendbeckens, Nordostbayern*, Schweizerbart
710 Science Publishers, Stuttgart, Germany, 1988.

711 Eberts, A., Fazlikhani, H., Bauer, W., Stollhofen, H., Wall, H. de, and Gabriel, G.: Late to post-Variscan
712 basement segmentation and differential exhumation along the SW Bohemian Massif, central
713 Europe, *Solid Earth*, 12, 2277–2301, <https://doi.org/10.5194/se-12-2277-2021>, available at:
714 <https://se.copernicus.org/articles/12/2277/2021/>, 2021.

715 Edel, J. B. and Weber, K.: Cadomian terranes, wrench faulting and thrusting in the central Europe
716 Variscides: geophysical and geological evidence, *Geologische Rundschau*, 84, 412–432,
717 <https://doi.org/10.1007/BF00260450>, 1995.

718 Ehling, B.-C. and Gebhardt, U.: Rotliegend im Saale-Becken, in: *Innervariscische Becken*, edited by:
719 Lützner, H., Schweizerbart Science Publishers, Stuttgart, Germany, 504–516, 2012.

720 Emmert, U., Gudden, H., Haunschild, H., Meyer, R. K. F., Schmid, H., Schuh, H., and Stettner, G.:
721 Bohrgut-Beschreibung der Forschungsbohrung Obernsees, *Geologica Bavarica*, 88, 23–47, 1985.

722 Engel, W., Feist, R., and Franke, W.: Le Carbonifère anté-Stéphanien de la Montagne Noire: rapports
723 entre mise en place des nappes et sédimentation., *Bulletin du BRGM*, 1, 341–389, 1982.

724 Fazlikhani, H. and Back, S.: The influence of differential sedimentary loading and compaction on the
725 development of a deltaic rollover, *Marine and Petroleum Geology*, 59, 136–149,
726 <https://doi.org/10.1016/j.marpetgeo.2014.08.005>, 2015.

727 Fazlikhani, H., Aagotnes, S. S., Refvem, M. A., Hamilton-Wright, J., Bell, R. E., Fossen, H., Gawthorpe,
728 R. L., Jackson, C. A.-L., and Rotevatn, A.: Strain migration during multiphase extension, Stord
729 Basin, northern North Sea rift, *Basin Res*, 33, 1474–1496, <https://doi.org/10.1111/bre.12522>,
730 2021.

731 Fazlikhani, H., Fossen, H., Gawthorpe, R. L., Faleide, J. I., and Bell, R. E.: Basement structure and its
732 influence on the structural configuration of the northern North Sea rift, *Tectonics*, 36, 1151–
733 1177, <https://doi.org/10.1002/2017TC004514>, 2017.

734 Festa, A., Balestro, G., Borghi, A., Caroli, S. de, and Succo, A.: The role of structural inheritance in
735 continental break-up and exhumation of Alpine Tethyan mantle (Canavese Zone, Western Alps),
736 *Geoscience Frontiers*, 11, 167–188, <https://doi.org/10.1016/j.gsf.2018.11.007>, available at:
737 <http://www.sciencedirect.com/science/article/pii/S1674987118302470>, 2020.

738 Fossen, H.: Extensional tectonics in the North Atlantic Caledonides: a regional view, *Geological*
739 *Society, London, Special Publications*, 335, 767, <https://doi.org/10.1144/SP335.31>, 2010.

740 Franke, W.: The mid-European segment of the Variscides: tectonostratigraphic units, terrane
741 boundaries and plate tectonic evolution, in: *Orogenic Processes: Quantification and Modelling in*
742 *the Variscan Belt*, edited by: Franke, W., Haak, V., Oncken, O., and Tanner, D. C., 35,
743 <https://doi.org/10.1144/GSL.SP.2000.179.01.05>, 2000.

744 Franke, W. and Stein, E.: Exhumation of high-grade rocks in the Saxo-Thuringian Belt: Geological
745 constraints and geodynamic concepts, in: *Orogenic Processes: Quantification and Modelling in*
746 *the Variscan Belt*, <https://doi.org/10.1144/GSL.SP.2000.179.01.20>, 2000.

747 Franke, W., Behrmann, J., and Moehrmann, H.: Zur Deformationsgeschichte des Kristallins im
748 Münchberger Deckenstapel, *KTB Report*, 92-4, 225–240, 1992.

749 Franke, W.: Tectonostratigraphic units in the Variscan belt of central Europe, in: *Terranes in the*
750 *Circum-Atlantic Paleozoic Orogens*, edited by: Dallmeyer, R. D., *Geological Society of America*, 0,
751 <https://doi.org/10.1130/SPE230-p67>, 1989.

752 Franke, W., Cocks, L. R. M., and Torsvik, T. H.: The Palaeozoic Variscan oceans revisited, *Gondwana*
753 *Research*, 48, 257–284, <https://doi.org/10.1016/j.gr.2017.03.005>, 2017.

754 Franke, W., Haak, V., Oncken, O., and Tanner, D. C. (Eds.): *Orogenic Processes: Quantification and*
755 *Modelling in the Variscan Belt*, 179, 2000.

756 Franz, M., Nowak, K., Berner, U., Heunisch, C., Bandel, K., Röhling, H.-G., and Wolfgramm, M.:
757 Eustatic control on epicontinental basins: The example of the Stuttgart Formation in the Central
758 European Basin (Middle Keuper, Late Triassic), *Global and Planetary Change*, 122, 305–329,
759 <https://doi.org/10.1016/j.gloplacha.2014.07.010>, available at:
760 <https://www.sciencedirect.com/science/article/pii/S092181811400143X>, 2014.

761 Freudenberger, W. and Schwerd, K.: Erläuterungen zur Geologischen Karte von Bayern 1. Geol.
762 :500000, Bayerisches Geologisches Landesamt, München, 1996.

763 Freudenberger, W., Herold, B., and Wagner, S.: Bohrkern-Beschreibung und Stratigraphie der
764 Forschungsbohrungen Lindau 1 und Spitzeichen 1, *Geologica Bavarica*, 109, 15–26, 2006.

765 Freyberg, B. von: Tektonische Karte der Fränkischen Alb und ihrer Umgebung, *Erlanger Geologische*
766 *Abhandlungen*, 77, 1–81, 1969.

767 Friedlein, V. and Hahn, T.: Mittelberg well description: Internal report, Bayerisches Landesamt fuer
768 Umwelt, 2018.

769 Gudden, H.: Der Untere Keuper in Bohrungen zwischen Eltmann und Rodach, *Geologische Blätter*
770 *von Nordost-Bayern*, 31, 448–462, 1981.

771 Gudden, H.: Die Thermal-Mineralwasser-Erschließungsbohrung Staffelstein 1975, *Brunnenbau, Bau*
772 *von Wasserwerken und Rohrleitungsbau (bbr)*, 28, 85–92, 1977.

773 Gudden, H. and Schmid, H.: Die Forschungsbohrung Obernsees—Konzeption, Durchführung und
774 Untersuchung der Metallführung, *Geologica Bavarica*, 88, 5–21, 1985.

775 Gudden, H.: Der Buntsandstein in der Forschungsbohrung Obernsees, *Geologica Bavarica*, 88, 69–81,
776 1985.

777 Gudden, H.: über die Struktur Mürsbach und ihre Eignung für behälterlose unterirdische
778 Gasspeicherung, München, 1971.

779 Hahn, T., Kroner, U., and Mezer, P.: Lower Carboniferous synorogenic sedimentation in the Saxo-
780 Thuringian Basin and the adjacent Allochthonous Domain, in: *Pre-Mesozoic geology of Saxo-*
781 *Thuringia: From the Cadomian active margin to the Variscan orogen*, edited by: Linnemann, U.
782 and Romer, R. L., Schweizerbart, Stuttgart, 171–192, 2010.

783 Hallas, P., Pfänder, J. A., Kroner, U., and Sperner, B.: Microtectonic control of $^{40}\text{Ar}/^{39}\text{Ar}$ white mica
784 age distributions in metamorphic rocks (Erzgebirge, N-Bohemian Massif): Constraints from
785 combined step heating and multiple single grain total fusion experiments, *Geochimica et*
786 *Cosmochimica Acta*, 314, 178–208, <https://doi.org/10.1016/j.gca.2021.08.043>, available at:
787 <https://www.sciencedirect.com/science/article/pii/S0016703721005329>, 2021.

788 Haunschild, H.: Der Keuper in der Forschungsbohrung Obernsees, *Geologica Bavarica*, 88, 103–130,
789 available at: https://www.lfu.bayern.de/geologie/geo_karten_schriften/schriften/index.htm,
790 1985.

791 Heilman, E., Kolawole, F., Atekwana, E. A., and Mayle, M.: Controls of Basement Fabric on the
792 Linkage of Rift Segments, *Tectonics*, 38, 1337–1366, <https://doi.org/10.1029/2018TC005362>,
793 2019.

794 Heinrichs, T., Giese, P., and Bankwitz, E.: DEKORP 3/MVE-90 (West) Preliminary geological
795 interpretation of a deep near-vertical reflection profile between the Rhenish and the Bohemian
796 Massifs, Germany, *Zeitschrift für Geologische Wissenschaften*, 22, 771–801, 1994.

797 Helmkampf, K. E.: Profilvergleich und sedimentologische Entwicklung im Umkreis der
798 Forschungsbohrungen Spitzeichen 1 und Lindau 1, *Geologica Bavarica*, 109, 63–94, 2006.

799 Helmkampf, K. E., Kuhlmann, J., and Kaiser, D.: Das Rotliegende im Bereich der Weidener Bucht, in:
800 *Geologica Bavarica 83: Neue Tiefbohrungen in Bayern*, edited by: Bayerisches Geologisches
801 Landesamt, Bayerisches Geologisches Landesamt, München, 167–186, 1982.

802 Henk, A.: Gravitational orogenic collapse vs plate-boundary stresses: a numerical modelling
803 approach to the Permo-Carboniferous evolution of Central Europe, *Geologische Rundschau*, 86,
804 39–55, <https://doi.org/10.1007/s005310050120>, 1997.

805 Henk, A.: Late orogenic Basin evolution in the Variscan internides: the Saar-Nahe Basin, southwest
806 Germany, *Tectonophysics*, 223, 273–290, [https://doi.org/10.1016/0040-1951\(93\)90141-6](https://doi.org/10.1016/0040-1951(93)90141-6),
807 available at: <https://www.sciencedirect.com/science/article/pii/0040195193901416>, 1993.

808 Herrmann, R.: Die stratigraphischen und tektonischen Verhältnisse des Stockheimer Beckens.,
809 *Geologie*, 7, 133–157, 1958.

810 Heuse, T., Blumenstengel, H., Elicki, O., Geyer, G., Hansch, W., Maletz, J., Sarmiento, G. N., and
811 Weyer, D.: Biostratigraphy - The faunal province of the southern margin of the Rheic Ocean, in:
812 *Pre-Mesozoic geology of Saxo-Thuringia: From the Cadomian active margin to the Variscan*
813 *orogen*, edited by: Linnemann, U. and Romer, R. L., Schweizerbart, Stuttgart, 99–170, 2010.

814 Hirschmann, G.: KTB — The structure of a Variscan terrane boundary: seismic investigation — drilling
815 — models, *Tectonophysics*, 264, 327–339, [https://doi.org/10.1016/S0040-1951\(96\)00171-0](https://doi.org/10.1016/S0040-1951(96)00171-0),
816 available at: <https://www.sciencedirect.com/science/article/pii/S0040195196001710>, 1996.

817 Kley, J. and Voigt, T.: Late Cretaceous intraplate thrusting in central Europe: Effect of Africa-Iberia-
818 Europe convergence, not Alpine collision, *Geology*, 36, 839–842,
819 <https://doi.org/10.1130/G24930A.1>, 2008.

820 Koehl, J.-B. P., Bergh, S. G., Henningsen, T., and Faleide, J. I.: Middle to Late Devonian–Carboniferous
821 collapse basins on the Finnmark Platform and in the southwesternmost Nordkapp basin, SW

822 Barents Sea, *Solid Earth*, 9, 341–372, <https://doi.org/10.5194/se-9-341-2018>, available at:
823 <https://www.solid-earth.net/9/341/2018/>, 2018.

824 Köhler, S., Duschl, F., Fazlikhani, H., Koehn, D., Stephan, T., and Stollhofen, H.: Reconstruction of
825 cyclic Mesozoic-Cenozoic stress development in SE Germany using fault-slip and stylolite
826 inversion, submitted to the *Geological Magazine*.

827 Kossmat, F.: Gliederung des varistischen Gebirgsbaues., *Abhandlungen des Sächsischen*
828 *Geologischen Landesamtes*, 1, 1–39, 1927.

829 Krohe, A.: Variscan tectonics of central Europe: Postaccretionary intraplate deformation of weak
830 continental lithosphere, *Tectonics*, 15, 1364–1388, <https://doi.org/10.1029/96TC01110>,
831 available at: <https://www.scopus.com/inward/record.uri?eid=2-s2.0-0030390295&doi=10.1029%2f96TC01110&partnerID=40&md5=a69bf89c67177c6a9a7d76d35a93aee5>, 1996.

832
833

834 Kroner, U., Hahn, T., Romer, R. L., and Linnemann, U.: The Variscan orogeny in the Saxo-Thuringian
835 zone—Heterogenous overprint of Cadomian/Paleozoic Peri-Gondwana crust, in: *The Evolution of*
836 *the Rheic Ocean: From Avalonian-Cadomian Active Margin to Alleghenian-Variscan Collision*,
837 edited by: Linnemann, U., Nance, R. D., Kraft, P., and Zulauf, G., *Geological Society of America*,
838 119, [https://doi.org/10.1130/2007.2423\(06\)](https://doi.org/10.1130/2007.2423(06)), 2007.

839 Kroner, U. and Goerz, I.: Variscan assembling of the Allochthonous Domain of the Saxo-Thuringian
840 Zone - a tectonic model, in: *Pre-Mesozoic geology of Saxo-Thuringia: From the Cadomian active*
841 *margin to the Variscan orogen*, edited by: Linnemann, U. and Romer, R. L., *Schweizerbart*,
842 *Stuttgart*, 271–286, 2010.

843 Laversanne, J.: Le Permian de Lodeve (Massif Central Francais). Evolution des depots Autuniens et
844 exemples de mineralisations uraniferes diagenetiques par circulation de solutions exogenes,
845 1978.

846 Leitz, F. and Schröder, B.: Die Randfazies der Trias und Bruchschollenland südöstlich Bayreuth
847 (Exkursion C am 11. und 12. April 1985), *Jahresberichte und Mitteilungen des Oberrheinischen*
848 *Geologischen Vereins*, 67, 51–63, <https://doi.org/10.1127/jmogv/67/1985/51>, 1985.

849 Lenhart, A., Jackson, C. A.-L., Bell, R. E., Duffy, O. B., Gawthorpe, R. L., and Fossen, H.: Structural
850 architecture and composition of crystalline basement offshore west Norway, *Lithosphere*, 11,
851 273–293, <https://doi.org/10.1130/L668.1>, 2019.

852 Linnemann, U. and Romer, R. L. (Eds.): *Pre-Mesozoic geology of Saxo-Thuringia: From the Cadomian*
853 *active margin to the Variscan orogen*, *Schweizerbart*, *Stuttgart*, 488 pp., 2010.

854 Linnemann, U. and Heuse, T.: The Ordovician of the Schwarzburg Anticline: Geotectonic setting,
855 biostratigraphy and sequence stratigraphy (Saxo-Thuringian Terrane, Germany), *Zeitschrift der*
856 *Deutschen Geologischen Gesellschaft*, 151, 471–491,
857 <https://doi.org/10.1127/zdgg/151/2001/471>, 2001.

858 Linnemann, U., Hofmann, M., Romer, R. L., and Gerdes, A.: Transitional stages between the
859 Cadomian and Variscan orogenies: Basin development and tectono-magmatic evolution of the
860 southern margin of the Rheic Ocean in the Saxo-Thuringian Zone (North Gondwana shelf), in:
861 *Pre-Mesozoic geology of Saxo-Thuringia: From the Cadomian active margin to the Variscan*
862 *orogen*, edited by: Linnemann, U. and Romer, R. L., *Schweizerbart*, *Stuttgart*, 59–98, 2010.

863 Lüschen, E., Wenzel, F., Sandmeier, K.-J., Menges, D., Rühl, T., Stiller, M., Janoth, W., Keller, F.,
864 Söllner, W., Thomas, R., Krohe, A., Stenger, R., Fuchs, K., Wilhelm, H., and Eisbacher, G.: Near-
865 vertical and wide-angle seismic surveys in the Black Forest, SW Germany, *Journal of Geophysics*,
866 62, 1–30, 1987.

867 Lützner, H., Andreas, D., Schneider, J. W., Voigt, S., and Werneburg, R.: *Stefan und Rotliegend im*
868 *Türinger Wald und seiner Umgebung*, in: *Innervariscische Becken*, edited by: Lützner, H.,
869 *Schweizerbart Science Publishers*, *Stuttgart*, *Germany*, 418–487, 2012.

870 Matter, A., Peters, T. J., Bläsi, H. R., and Ziegler, H. J.: Sondierbohrung Riniken, in: NAGRA
871 Technischer Bericht, 1–214, 1987.

872 McCann, T., Pascal, C., Timmerman, M. J., Krzywiec, P., López-Gómez, J., Wetzel, L., Krawczyk, C. M.,
873 Rieke, H., and Lamarche, J.: Post-Variscan (end Carboniferous–Early Permian) basin evolution in
874 Western and Central Europe, Geological Society, London, Memoirs, 32, 355–388,
875 <https://doi.org/10.1144/GSL.MEM.2006.032.01.22>, 2006.

876 Meissner, R., Wever, T., and Bittner, R.: Results of DEKORP 2-S and other reflection profiles through
877 the Variscides, *Geophys J Int*, 89, 319–324, <https://doi.org/10.1111/j.1365-246X.1987.tb04425.x>,
878 1987.

879 Müller, M.: Neue Vorstellungen zur Entwicklung des Nordostbayerischen Permokarbon-Trogs
880 aufgrund reflexionsseismischer Messungen in der Mittleren Oberpfalz, *Geologische Blätter von*
881 *Nordost-Bayern*, 44, 195–224, 1994.

882 Navabpour, P., Malz, A., Kley, J., Siegburg, M., Kasch, N., and Ustaszewski, K.: Intraplate brittle
883 deformation and states of paleostress constrained by fault kinematics in the central German
884 platform, *Tectonophysics*, 694, 146–163, <https://doi.org/10.1016/j.tecto.2016.11.033>, 2017.

885 Norton, M. G., McClay, K. R., and Way, N. A.: Tectonic evolution of Devonian basins in northern
886 Scotland and southern Norway, *NJG*, 67, 323–338, available at: [http://njg.geologi.no/vol-61-](http://njg.geologi.no/vol-61-70/details/19/712-712)
887 [70/details/19/712-712](http://njg.geologi.no/vol-61-70/details/19/712-712), 1987.

888 Osagiede, E. E., Rotevatn, A., Gawthorpe, R., Kristensen, T. B., Jackson, C. A.-L., and Marsh, N.: Pre-
889 existing intra-basement shear zones influence growth and geometry of non-colinear normal
890 faults, western Utsira High–Heimdal Terrace, North Sea, *Geol*, 103908,
891 <https://doi.org/10.1016/j.jsg.2019.103908>, available at:
892 <http://www.sciencedirect.com/science/article/pii/S0191814119301798>, 2019.

893 Osmundsen, P. T. and Andersen, T. B.: The middle Devonian basins of western Norway: sedimentary
894 response to large-scale transtensional tectonics?, *Tectonophysics*, 332, 51–68,
895 [https://doi.org/10.1016/S0040-1951\(00\)00249-3](https://doi.org/10.1016/S0040-1951(00)00249-3), available at:
896 <https://www.sciencedirect.com/science/article/pii/S0040195100002493>, 2001.

897 Patruno, S., Reid, W., Berndt, C., and Feuilleaubois, L.: Polyphase tectonic inversion and its role in
898 controlling hydrocarbon prospectivity in the Greater East Shetland Platform and Mid North Sea
899 High, UK, Geological Society, London, Special Publications, 471, 177,
900 <https://doi.org/10.1144/SP471.9>, 2019.

901 Paul, J.: Rotliegend und unterer Zechstein der Forschungsbohrung Lindau 1 (NE-Bayern), *Geologica*
902 *Bavarica*, 109, 27–48, 2006.

903 Paul, J. and Schröder, B.: Rotliegend im Ostteil der Süddeutschen Scholle, in: *Innervariscische*
904 *Becken*, edited by: Lütznert, H., Schweizerbart Science Publishers, Stuttgart, Germany, 697–706,
905 2012.

906 Peace, A., McCaffrey, K., Imber, J., van Hunen, J., Hobbs, R., and Wilson, R.: The role of pre-existing
907 structures during rifting, continental breakup and transform system development, offshore West
908 Greenland, *Basin Res*, 30, 373–394, <https://doi.org/10.1111/bre.12257>, 2018.

909 Peterek, A., Rauche, H., Schröder, B., Franzke, H.-J., Bankwitz, P., and Bankwitz, E.: The late-and post-
910 Variscan tectonic evolution of the Western Border fault zone of the Bohemian massif (WBZ),
911 *Geologische Rundschau*, 86, 191–202, <https://doi.org/10.1007/s005310050131>, available at:
912 <https://doi.org/10.1007/s005310050131>, 1997.

913 Peterek, A., Rauche, H., and Schröder, B.: Die strukturelle Entwicklung des E-Randes der
914 Süddeutschen Scholle in der Kreide, *Zeitschrift für Geologische Wissenschaften*, 24, 65–77,
915 1996a.

916 Peterek, A., Schröder, B., and Menzel, D.: Zur postvariszischen Krustenentwicklung des Naabgebirges
917 und seines Rahmens, *Zeitschrift für Geologische Wissenschaften*, 24, 293–304, 1996b.

918 Peterek, A., Schröder, B., and Menzel, D.: Zur postvariszischen Krustenentwicklung des Naabgebirges
919 und seines Rahmens, *Zeitschrift für Geologische Wissenschaften*, 24, 293–304, 1996c.

920 Phillips, T. B. and McCaffrey, K. J. W.: Terrane Boundary Reactivation, Barriers to Lateral Fault
921 Propagation and Reactivated Fabrics: Rifting Across the Median Batholith Zone, Great South
922 Basin, New Zealand, *Tectonics*, 38, 4027–4053, <https://doi.org/10.1029/2019TC005772>, 2019.

923 Phillips, T. B., Fazlikhani, H., Gawthorpe, R. L., Fossen, H., Jackson, C. A.-L., Bell, R. E., Faleide, J. I.,
924 and Rotevatn, A.: The Influence of Structural Inheritance and Multiphase Extension on Rift
925 Development, the Northern North Sea, *Tectonics*, n/a, <https://doi.org/10.1029/2019TC005756>,
926 2019.

927 Phillips, T. B., Jackson, C. A.-L., Bell, R. E., Duffy, O. B., and Fossen, H.: Reactivation of intrabasement
928 structures during rifting: A case study from offshore southern Norway, *Journal of Structural
929 Geology*, 91, 54–73, <https://doi.org/10.1016/j.jsg.2016.08.008>, 2016.

930 Platt, N. H. and Cartwright, J. A.: Structure of the East Shetland Platform, northern North Sea,
931 *Petroleum Geoscience*, 4, 353, <https://doi.org/10.1144/petgeo.4.4.353>, 1998.

932 Ravidà, D. C. G., Caracciolo, L., Henares, S., Janßen, M., and Stollhofen, H.: Drainage and
933 environmental evolution across the Permo–Triassic boundary in the south-east Germanic Basin
934 (north-east Bavaria), *Sedimentology*, n/a, <https://doi.org/10.1111/sed.12913>, 2021.

935 Ring, U.: The influence of preexisting structure on the evolution of the Cenozoic Malawi rift (East
936 African rift system), *Tectonics*, 13, 313–326, <https://doi.org/10.1029/93TC03188>, 1994.

937 Schönig, J., Eynatten, H. von, Meinhold, G., Lünsdorf, N. K., Willner, A. P., and Schulz, B.: Deep
938 subduction of felsic rocks hosting UHP lenses in the central Saxonian Erzgebirge: Implications for
939 UHP terrane exhumation, *Gondwana Research*, 87, 320–329,
940 <https://doi.org/10.1016/j.gr.2020.06.020>, available at:
941 <https://www.sciencedirect.com/science/article/pii/S1342937X20302136>, 2020.

942 Schröder, B.: Outline of the Permo–Carboniferous Basins at the Western Margin of the Bohemian
943 Massif, *Zeitschrift für Geologische Wissenschaften*, 16, 993–1001, 1988.

944 Schröder, B.: Inversion tectonics along the Western margin of the Bohemian Massif, *Tectonophysics*,
945 137, 93–100, [https://doi.org/10.1016/0040-1951\(87\)90316-7](https://doi.org/10.1016/0040-1951(87)90316-7), available at:
946 <http://www.sciencedirect.com/science/article/pii/0040195187903167>, 1987.

947 Schuh, H.: Der Zechstein in der Forschungsbohrung Obernsees, *Geologica Bavarica*, 88, 57–68, 1985.

948 Schwan, W.: Die sächsischen Zwischengebirge und Vergleiche mit der Münchberger Gneismasse und
949 anderen analogen Kristallinvorkommen im Saxothuringikum, *Erlanger geologische
950 Abhandlungen*, Heft 99, Erlangen: s.n, 180 p. 11 leaves of plates, 1974.

951 Swan, W.: Die Sächsischen Zwischengebirge und Vergleiche mit der Münchberger Gneismasse und
952 anderen analogen Kristallinvorkommen im Saxothuringikum., *Erlanger geologische
953 Abhandlungen*, 99, 1974.

954 Séranne, M.: Devonian extensional tectonics versus Carboniferous inversion in the northern
955 Orcadian basin, *Journal of the Geological Society*, 149, 27,
956 <https://doi.org/10.1144/gsjgs.149.1.0027>, 1992.

957 Séranne, M. and Séguret, M.: The Devonian basins of western Norway: tectonics and kinematics of
958 an extending crust, *Geological Society, London, Special Publications*, 28, 537,
959 <https://doi.org/10.1144/GSL.SP.1987.028.01.35>, 1987.

960 Sitting, E. and Nitsch, E.: Stefan und Rotliegend zwischen Odenwald und Alpenrand, in:
961 *Innervariscische Becken*, edited by: Lütznier, H., Schweizerbart Science Publishers, Stuttgart,
962 Germany, 646–696, 2012.

963 Specht, S.: Eltmann well description: Internal report, Bayerisches Landesamt fuer Umwelt, 2018.

964 Stephan, T., Kroner, U., Hahn, T., Hallas, P., and Heuse, T.: Fold/cleavage relationships as indicator
965 for late Variscan sinistral transpression at the Rheno-Hercynian–Saxo-Thuringian boundary zone,

966 Central European Variscides, *Tectonophysics*, 681, 250–262,
967 <https://doi.org/10.1016/j.tecto.2016.03.005>, available at:
968 <http://www.sciencedirect.com/science/article/pii/S004019511600161X>, 2016.

969 Stephenson, R. A., Narkiewicz, M., Dadlez, R., van Wees, J.-D., and Andriessen, P.: Tectonic
970 subsidence modelling of the Polish Basin in the light of new data on crustal structure and
971 magnitude of inversion, *Sedimentary Geology*, 156, 59–70, [https://doi.org/10.1016/S0037-](https://doi.org/10.1016/S0037-0738(02)00282-8)
972 [0738\(02\)00282-8](https://doi.org/10.1016/S0037-0738(02)00282-8), available at:
973 <https://www.sciencedirect.com/science/article/pii/S0037073802002828>, 2003.

974 Stettner, G.: Metamorphism and Tectonics in the Münchberg Mass and the Fichtelgebirge,
975 *Fortschritte der Mineralogie*, 52, 59–69, 1974.

976 Stettner, G. and Salger, M.: Das Schiefergebirge in der Forschungsbohrung Obernsees, *Geologica*
977 *Bavarica*, 88, 49–55, 1985.

978 Stollhofen, H.: Facies architecture variations and seismogenic structures in the Carboniferous–
979 Permian Saar–Nahe Basin (SW Germany): evidence for extension-related transfer fault activity,
980 *Sedimentary Geology*, 119, 47–83, [https://doi.org/10.1016/S0037-0738\(98\)00040-2](https://doi.org/10.1016/S0037-0738(98)00040-2), available at:
981 <https://www.sciencedirect.com/science/article/pii/S0037073898000402>, 1998.

982 Strugale, M., Da Schmitt, R. S., and Cartwright, J.: Basement geology and its controls on the
983 nucleation and growth of rift faults in the northern Campos Basin, offshore Brazil, *Basin Res*, n/a,
984 <https://doi.org/10.1111/bre.12540>, 2021.

985 Trusheim, F.: Über den Untergrund Frankens; Ergebnisse von Tief Bohrungen in Franken und
986 Nachbargebieten, *Geologica Bavarica*, 54, 1–106, 1964.

987 Vasconcelos, D. L., Bezerra, F. H., Medeiros, W. E., Castro, D. L. de, Clausen, O. R., Vital, H., and
988 Oliveira, R. G.: Basement fabric controls rift nucleation and postrift basin inversion in the
989 continental margin of NE Brazil, *Tectonophysics*, 751, 23–40,
990 <https://doi.org/10.1016/j.tecto.2018.12.019>, 2019.

991 Vetti, V. V. and Fossen, H.: Origin of contrasting Devonian supradetachment basin types in the
992 Scandinavian Caledonides, *Geology*, 40, 571–574, <https://doi.org/10.1130/G32512.1>, 2012.

993 Wagner, G. A., Coyle, D. A., Duyster, J., Henjes-Kunst, F., Peterek, A., Schröder, B., Stöckert, B.,
994 Wemmer, K., Zulauf, G., Ahrendt, H., Bischoff, R., Hejl, E., Jacobs, J., Menzel, D., Lal, N., van den
995 Haute, P., Vercoetere, C., and Welzel, B.: Post-Variscan thermal and tectonic evolution of the KTB
996 site and its surroundings, *J. Geophys. Res.*, 102, 18221–18232,
997 <https://doi.org/10.1029/96JB02565>, 1997.

998 Wemmer, K.: K-Ar-Altersdatierungsmöglichkeiten für retrograde Deformationsprozesse im spröden
999 und duktilen Bereich-Beispiele aus der KTB -Vorbohrung (Oberpfalz) und dem Bereich der
1000 Insubrischen Linie (N-Italien)., *Göttinger Arbeiten Zur Geologie und Paläontologie*, 51, 1–61,
1001 1991.

1002 Wever, T., Meissner, R., and Sadowiak, P.: Deep reflection seismic data along the central part of the
1003 European Geotraverse in Germany: a review, *Tectonophysics*, 176, 87–101,
1004 [https://doi.org/10.1016/0040-1951\(90\)90260-F](https://doi.org/10.1016/0040-1951(90)90260-F), available at:
1005 <http://www.sciencedirect.com/science/article/pii/004019519090260F>, 1990.

1006 Wiest, J. D., Wrona, T., Bauck, M. S., Fossen, H., Gawthorpe, R. L., Osmundsen, P. T., and Faleide, J. I.:
1007 From Caledonian Collapse to North Sea Rift: The Extended History of a Metamorphic Core
1008 Complex, *Tectonics*, 39, e2020TC006178, <https://doi.org/10.1029/2020TC006178>, 2020.

1009 Wrona, T., Fossen, H., Lecomte, I., Eide, C. H., and Gawthorpe, R. L.: Seismic expression of shear
1010 zones: Insights from 2-D point-spread-function-based convolution modelling, *Geol*, 104121,
1011 <https://doi.org/10.1016/j.jsjg.2020.104121>, available at:
1012 <http://www.sciencedirect.com/science/article/pii/S0191814119303037>, 2020.

1013 Ye, Q., Mei, L., Shi, H., Du, J., Deng, P., Shu, Y., and Camanni, G.: The Influence of Pre-existing
1014 Basement Faults on the Cenozoic Structure and Evolution of the Proximal Domain, Northern
1015 South China Sea Rifted Margin, *Tectonics*, 39, e2019TC005845,
1016 <https://doi.org/10.1029/2019TC005845>, 2020.
1017 Ziegler, P. A.: Tectonic and palaeogeographic development of the North Sea rift system, *Tectonic
1018 Evolution of North Sea Rifts*, 1–36, 1990.
1019
1020

1021 **Figure and Table caption**

1022
1023 **Figure 1:** Location of the study area in the Saxothuringian zone of Variscan orogeny. FRANKEN seismic
1024 survey is projected on geological map of the study area in dark red creating a grid of 2D seismic profiles
1025 with existing DEKORP profiles. Main Faults are shown as bold dark lines. Inset map shows exposed
1026 Variscan terranes in Central Europe. Yellow circles show deep wells in the study area. FRA: FRANKEN,
1027 MGCH: Mid German Crystalline High, FFS: Franconian Fault System and MN: Münchberg Nappe.
1028

1029 **Figure 2:** Velocity and density logs from well Mürsbach 1 utilized for synthetic seismogram generation.
1030 Seismic traces from FRANKEN-1802 are compared with generated synthetic seismogram. Velocity data
1031 are used to construct time-depth relationship and well-seismic ties. Depth to the formation tops are
1032 time converted and used as starting point for seismic interpretation.
1033

1034 **Figure 3:** Seismo-stratigraphic facies of observed Permian-Jurassic stratigraphy in the study area. A)
1035 Jurassic, B) Upper Triassic Keuper Group, c) Middle Triassic Muschelkalk Group, D) Lower Triassic
1036 Buntsandstein Group and D) Permian Zechstein and Rotliegend Groups.
1037

1038 **Figure 4:** Basement Seismic Facies (BSF) described along FRANKEN seismic survey. A) shows SE portion
1039 of FRANKEN-1804 below the Top Zechstein horizon. B) Low-amplitude and discontinuous reflections
1040 of BSF1 interpreted as Paleozoic metasedimentary rocks and Variscan nappe units. C) BSF2 shows
1041 high-amplitude, continuous and dipping reflection interpreted as Variscan shear zones. D) Medium-
1042 amplitude and semi-continuous reflections of BSF3 below Variscan shear zone related to the
1043 Cadomian basement and Paleozoic Inner shelf facies not involved in Variscan tectonics.
1044

1045 **Figure 5:** Reprocessed DEKORP-85 4N and DEKORP-3/MVE-90 profiles used to compare three
1046 Basement Seismic Facies (BSF1-3) described along FRANKEN seismic survey (see Fig. 1 for location).
1047 DEKORP profiles image exposed Variscan units along the western Bohemian Massif and are used as
1048 proxy for geological interpretation of BSFs. A) DEKORP-85 4N shows seismic signature of Paleozoic
1049 low-grade metasedimentary rocks (zoomed in B) and Münchberg Nappe (Variscan allochthon, zoomed
1050 in C) exposed at the surface and described as BSF1. D) DEKORP-3/MVE-90 images Münchberg nappe
1051 units east and Permian-Jurassic sedimentary cover west of Franconian Fault System (FFS). E) shows
1052 seismic signature of Variscan nappes (BSF1) and underlying shear zones (BSF2).
1053

1054 **Figure 6:** A) uninterpreted and B) interpreted FRANKEN-1801 profile. Horizon interpretation is tied to
1055 drilled wells in the study area. C) geo-seismic section in time (ms TWT), and D) depth converted profile
1056 with no vertical exaggeration. Intersecting profiles FRANKEN 1802 and 1804 are shown by black
1057 arrows. See Figure 1 for the profile location.
1058

1059 **Figure 7:** Profile FRANKEN-1802 strikes NE-SW, perpendicular to main structures. A) uninterpreted and
1060 B) interpreted seismic profile. FRANKEN-1802 is tied to well Eltmann, Mürsbach, Staffelstein 1 and 2.
1061 High-amplitude and continuous reflection of BSF2 interpreted as Variscan shear zones are at 2000-
1062 2500 ms TWT (5-6.5 km) in the NE and reach to the base of Permian sedimentary rocks to the SE. C)

1063 geo-seismic section in time with vertical exaggeration of 5. D) depth converted section with no vertical
1064 exaggeration. See Figure 1 for the profile location.

1065
1066 **Figure 8:** SE-NW striking FRANKEN-1803 profile, sub-parallel to the profile FRANKEN-1801. Horizon
1067 interpretation is tied to well Obernsees and intersection FRANKEN 1801 and 1804 profiles. A)
1068 uninterpreted and B) interpreted profile. C) geo-seismic section in time and D) depth converted
1069 section with not vertical exaggeration. Interpreted Variscan shear zones (BSF2) are at 2000-3000 ms
1070 (5-7 km) in the SE and reaches to ca. 2.5 km depth towards NW.

1071
1072 **Figure 9:** A) uninterpreted and B) interpreted profile FRANKEN-1804. Horizon interpretation along this
1073 profile is tied to intersection profiles FRANKEN 1801 and 1803. Note onlapping reflections in the
1074 hanging wall of SW-dipping normal faults creating Permian half-grabens. C) geo-seismic section in time
1075 and D) depth converted section with no vertical exaggeration. See Figure 1 for the profile location.

1076
1077 **Figure 10:** Present day three-dimensional view of interpreted Variscan units and structures west of
1078 Franconian Fault System (FFS). Variscan shear zone shows syn and antiformal geometries shallowing
1079 and thinning toward the W-SW.

1080
1081 **Figure 11:** Simplified and generic cartoons showing the relationships between orogenic structures and
1082 post-orogenic fault and basin development (note that shown general W-directed tectonic transport
1083 refers to the initial W-SW directed nappe stacking). At the latest orogenic and early post-orogenic
1084 period, normal faults develop in response to the regional stress field, some sub-parallel to the
1085 preexisting orogenic structures. Some of the normal faults grow laterally and vertically detaching into
1086 the underlying shear zones and initiate graben and half-graben basins in their hanging wall side.
1087 Normal faults not detaching into preexisting shear zones abandon.. After a Triassic and Jurassic
1088 regional tectonic quiescence, Cretaceous inversion event in Central Europe selectively reactivate
1089 Permian normal faults as steep reverse faults, exposing older stratigraphy in the hingingwall side and
1090 creating local syn and anticlines in the vicinity of reactivated faults.

1091
1092 **Figure 12:** Cartoon showing the relationship between shear zone geometry and fault development.
1093 Dark red area in the center shows folded part of the shear zone, where Lichtenfels Fault portion
1094 detaches into and is exposed at the surface. Laterally to the SW, shear zone is rather flat and
1095 Lichtenfels fault does not detach into and it is not exposed at the surface.

1096
1097 **Table 1:** Deep wells in the study area with formation tops used in seismic horizon interpretation of
1098 FRANKEN seism survey. See figure 1 for well location.

1099
1100 **Table 2:** Recording parameters of FRNAKEN seismic survey.

1101
1102
1103
1104

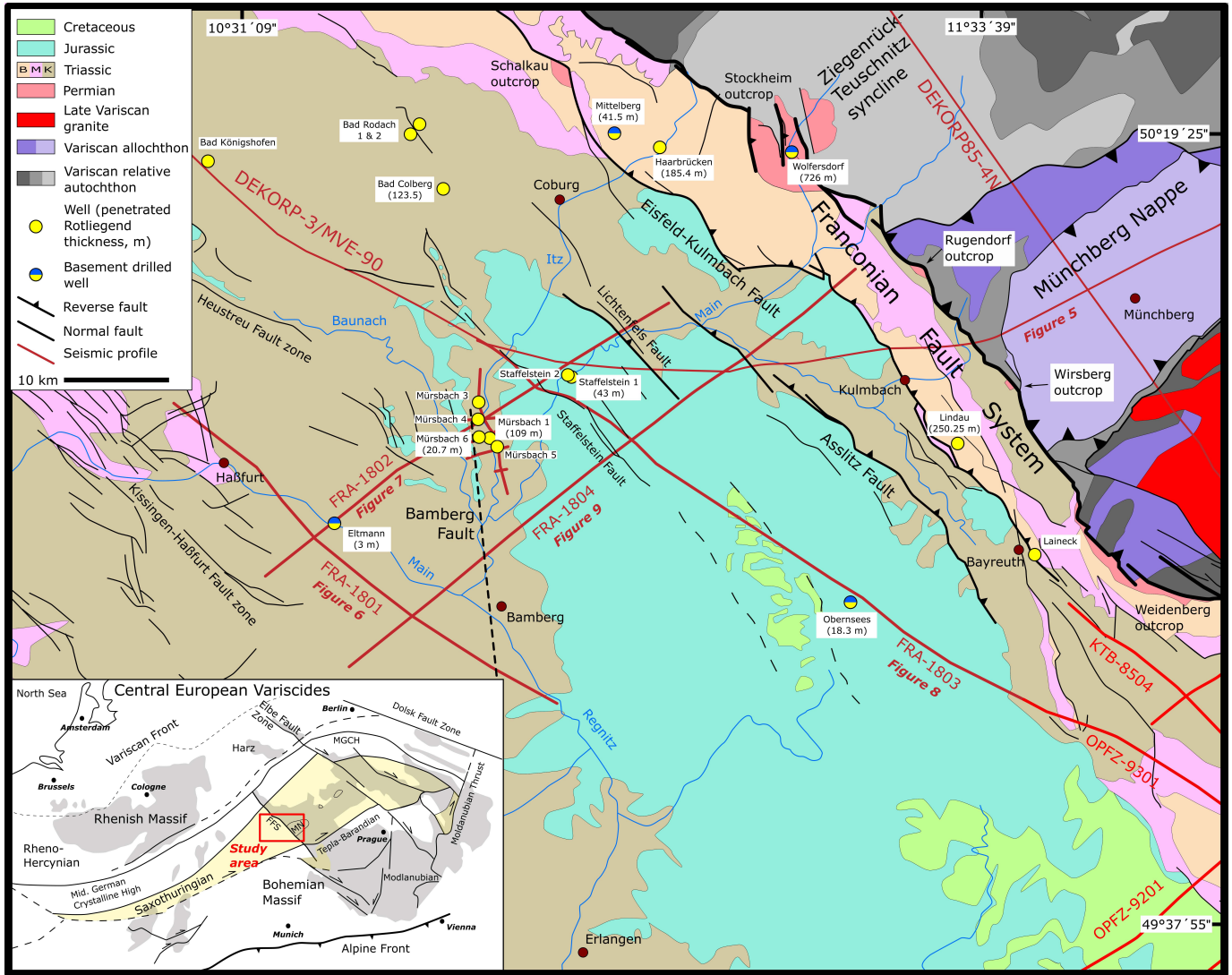


Figure 01

Well Mürsbach 1

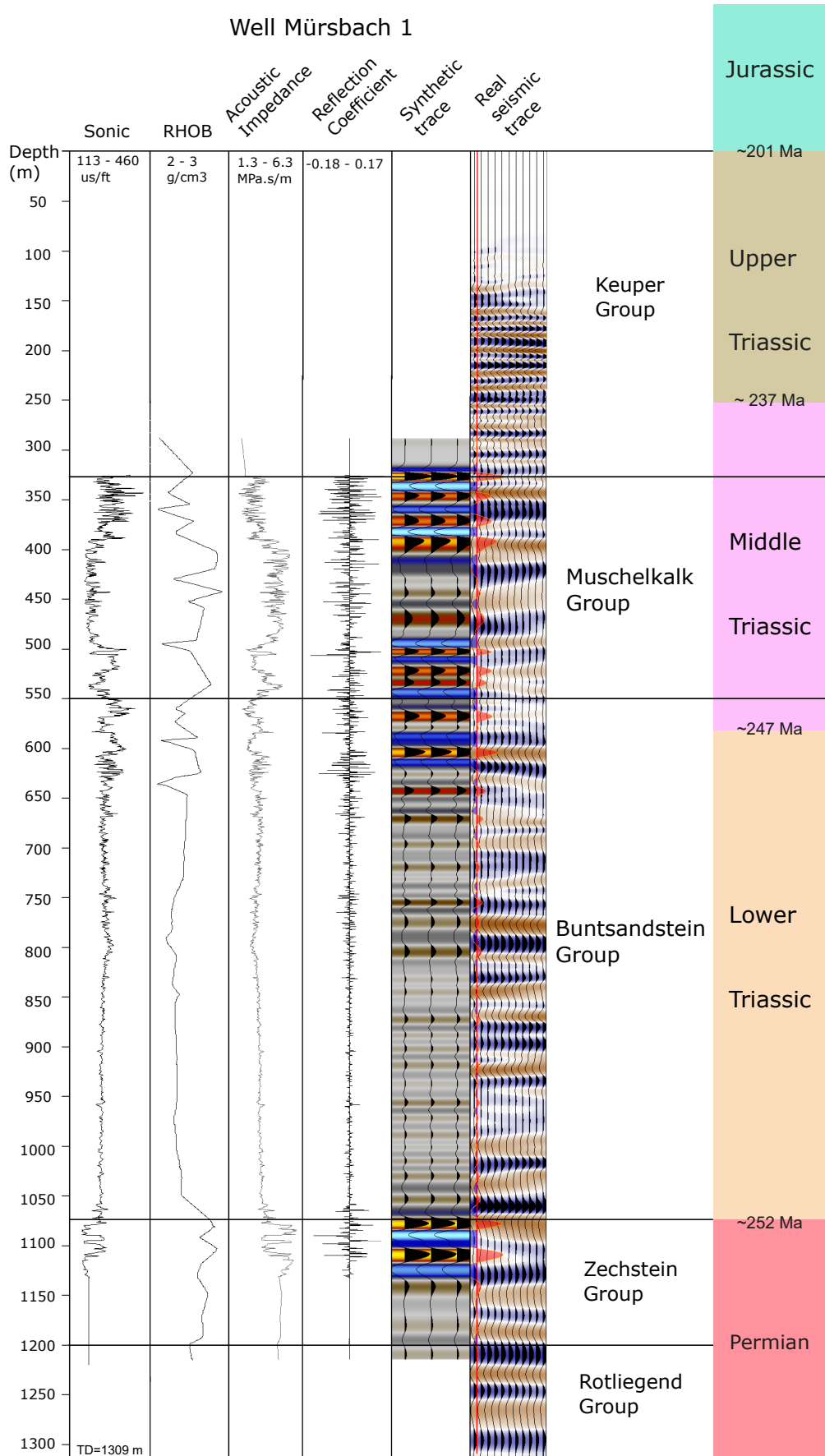


Figure 02

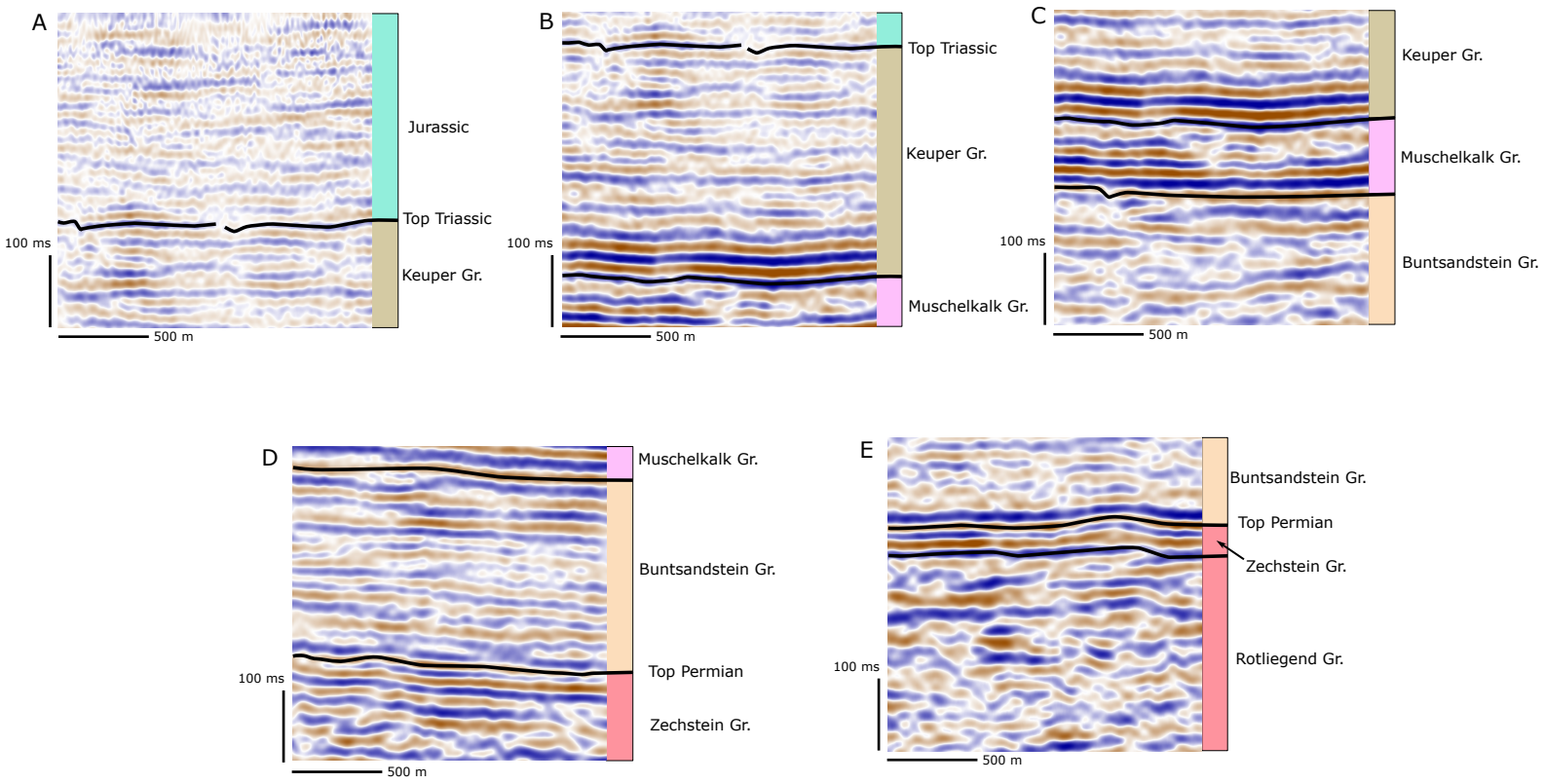
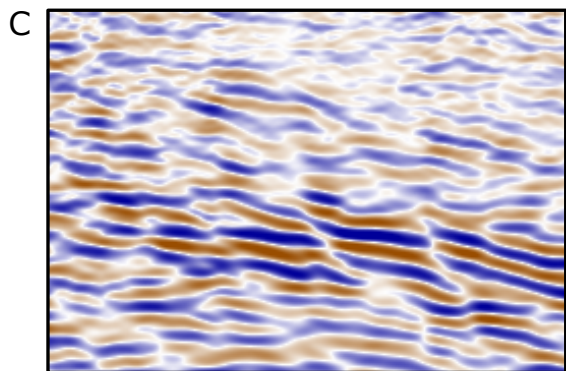
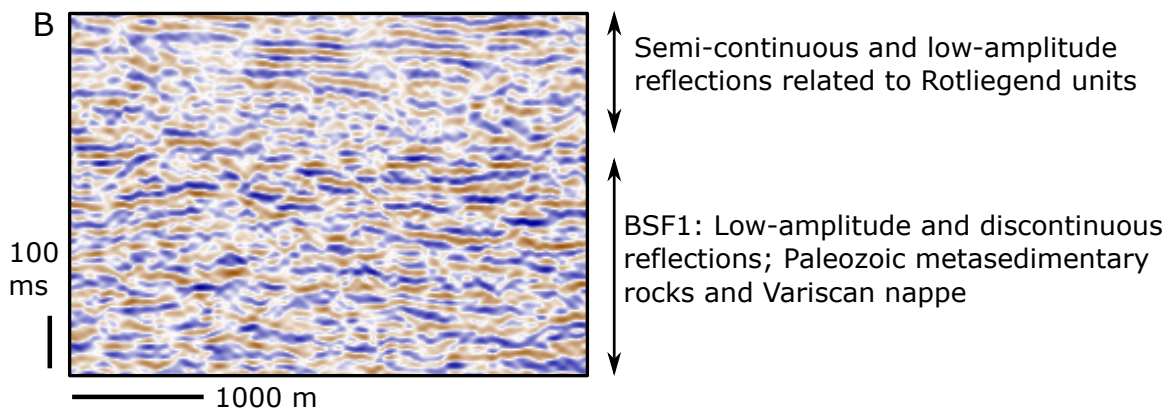
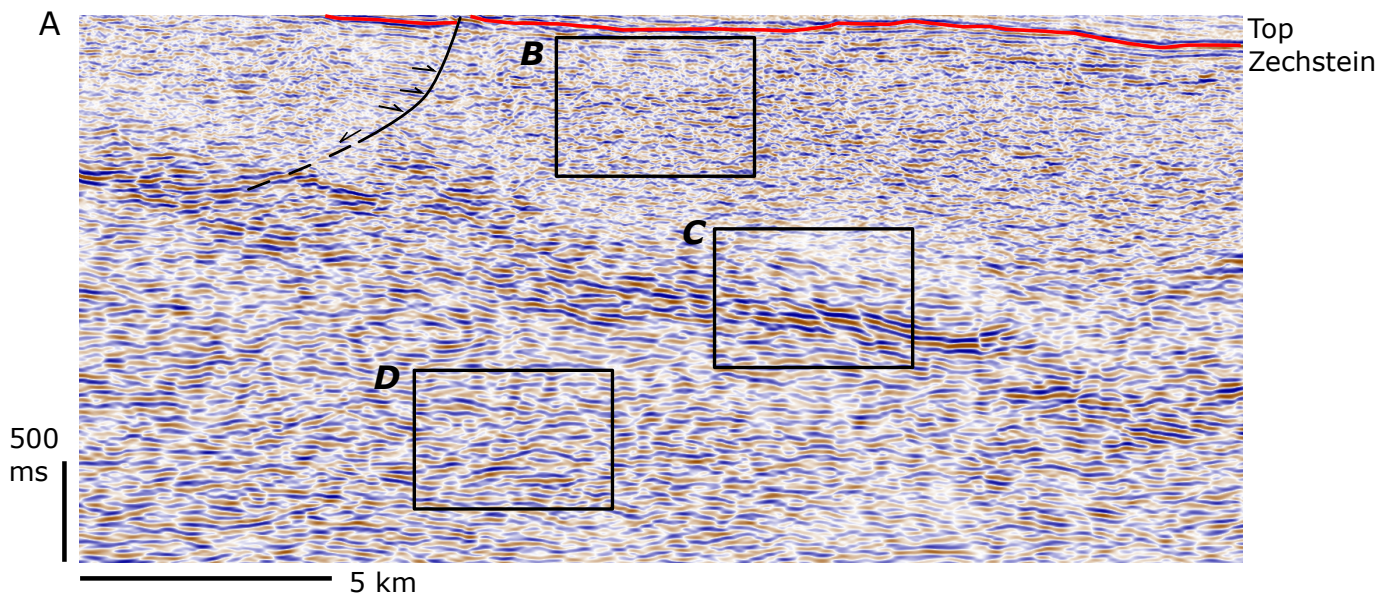
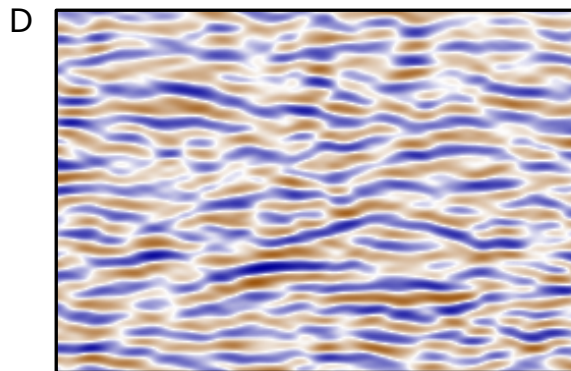


Figure 03



BSF2: High-amplitude and continuous reflections; Variscan shear zone



BSF3: Medium-amplitude and semi-continuous reflections; Cadomian basement and overlaying Paleozoic sequences

Figure 04

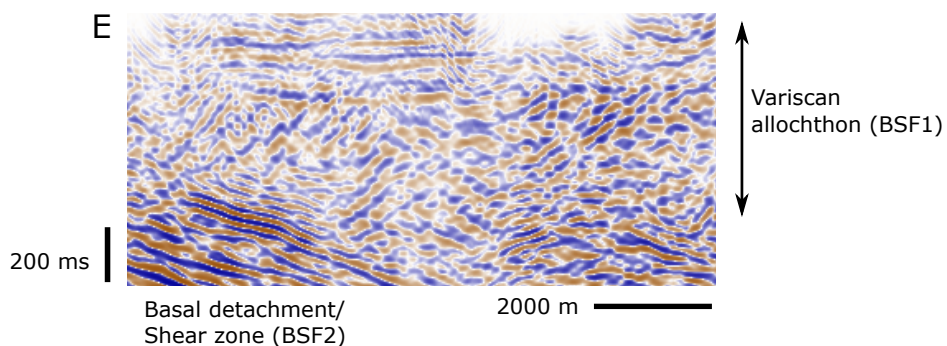
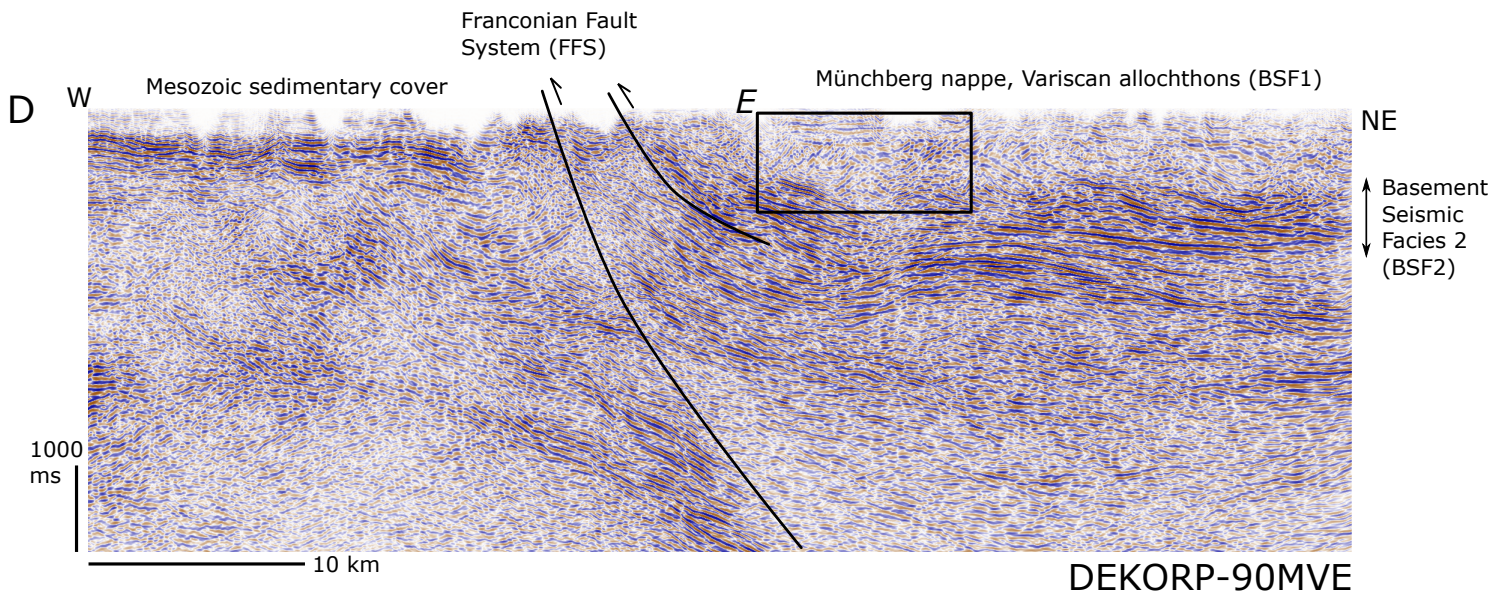
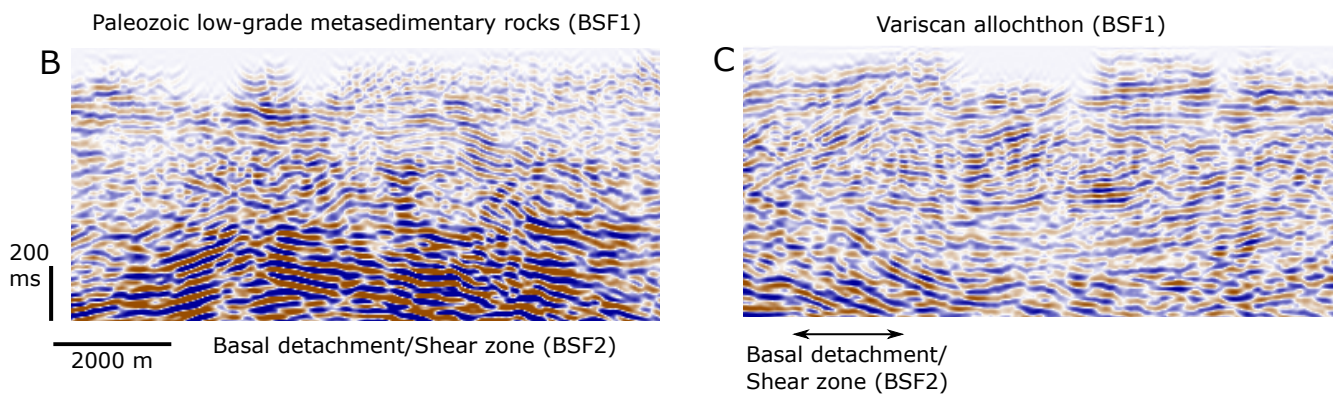
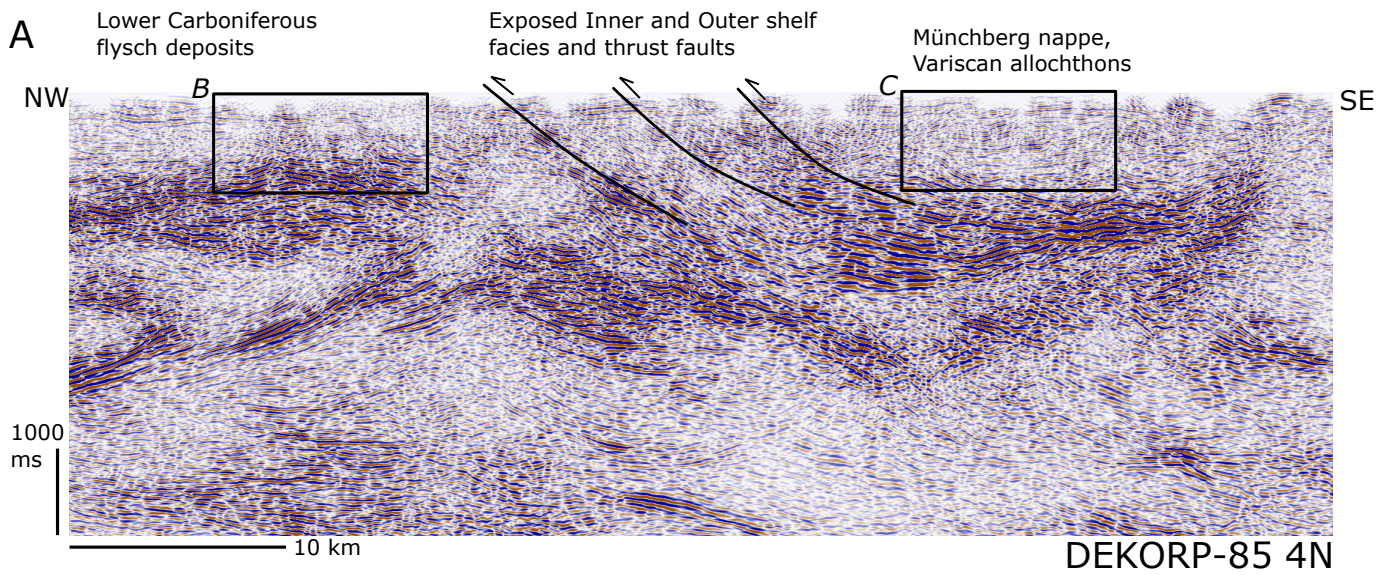


Figure 05

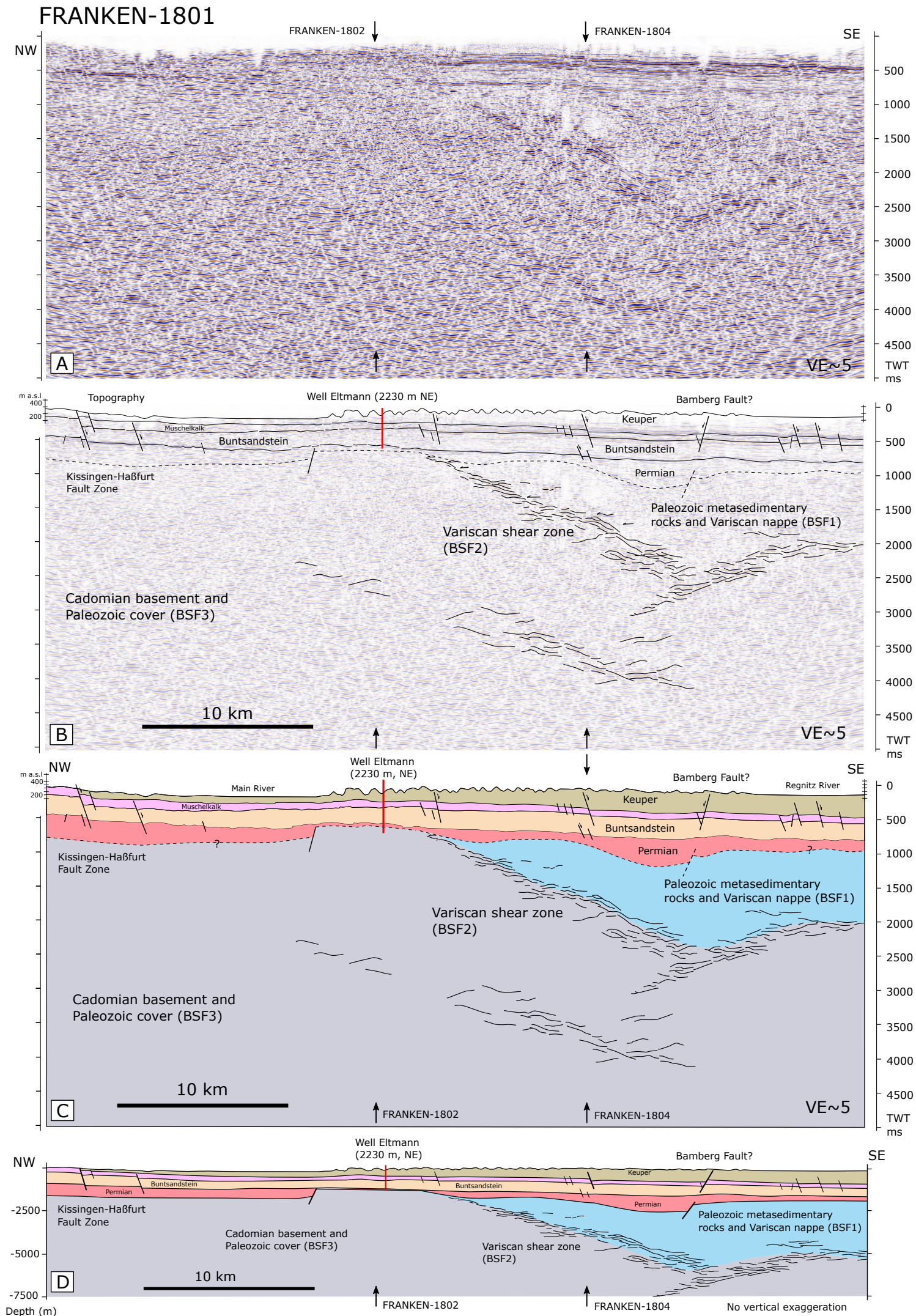


Figure 06

FRANKEN-1802

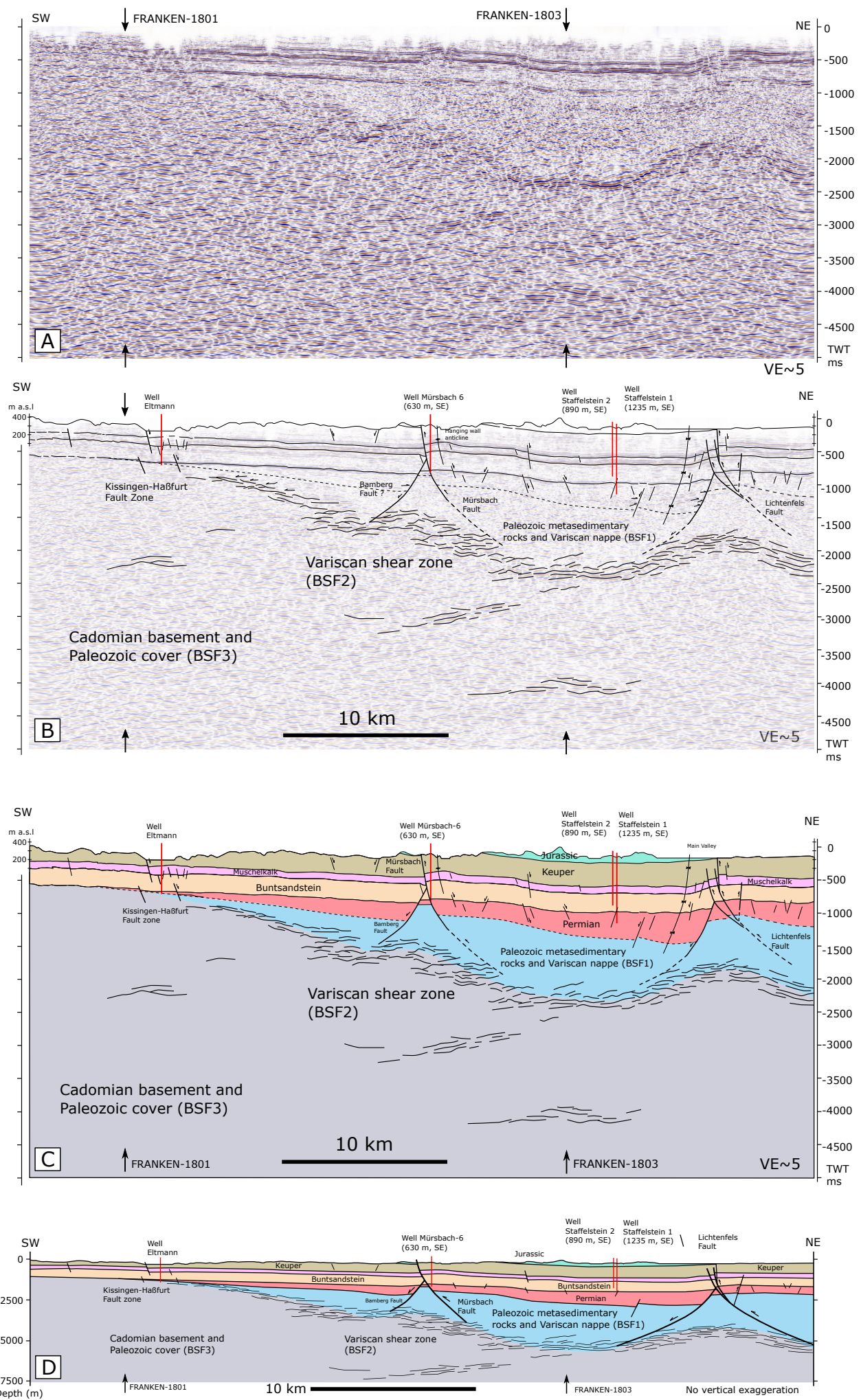


Figure 07

FRANKEN-1803

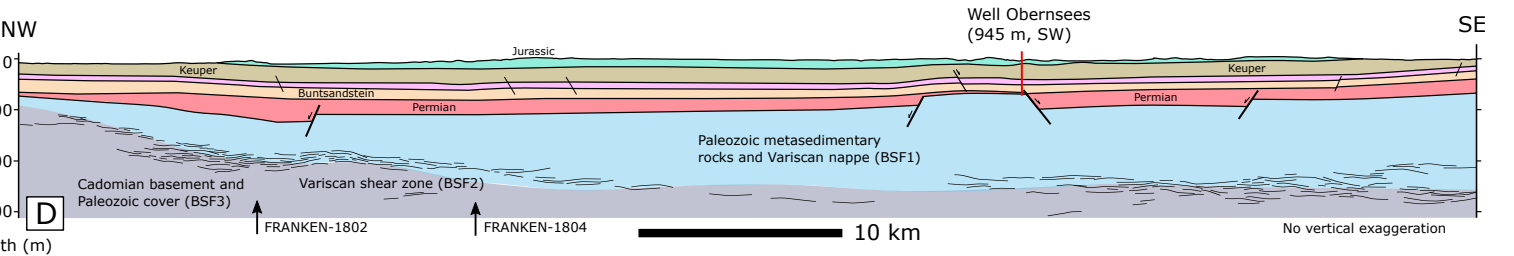
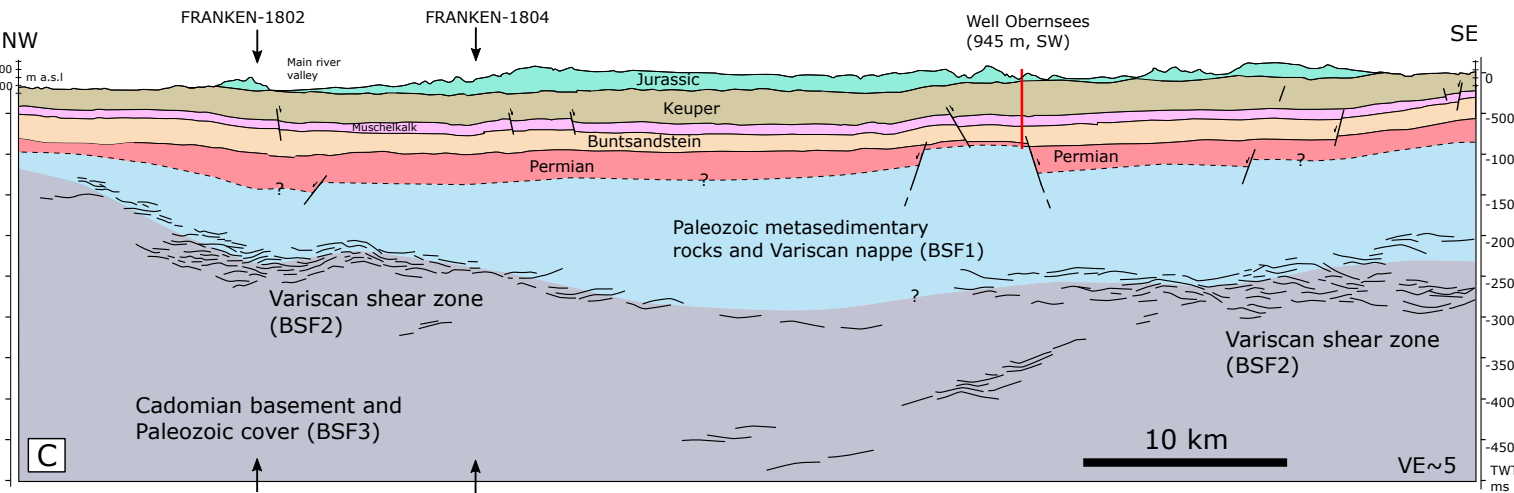
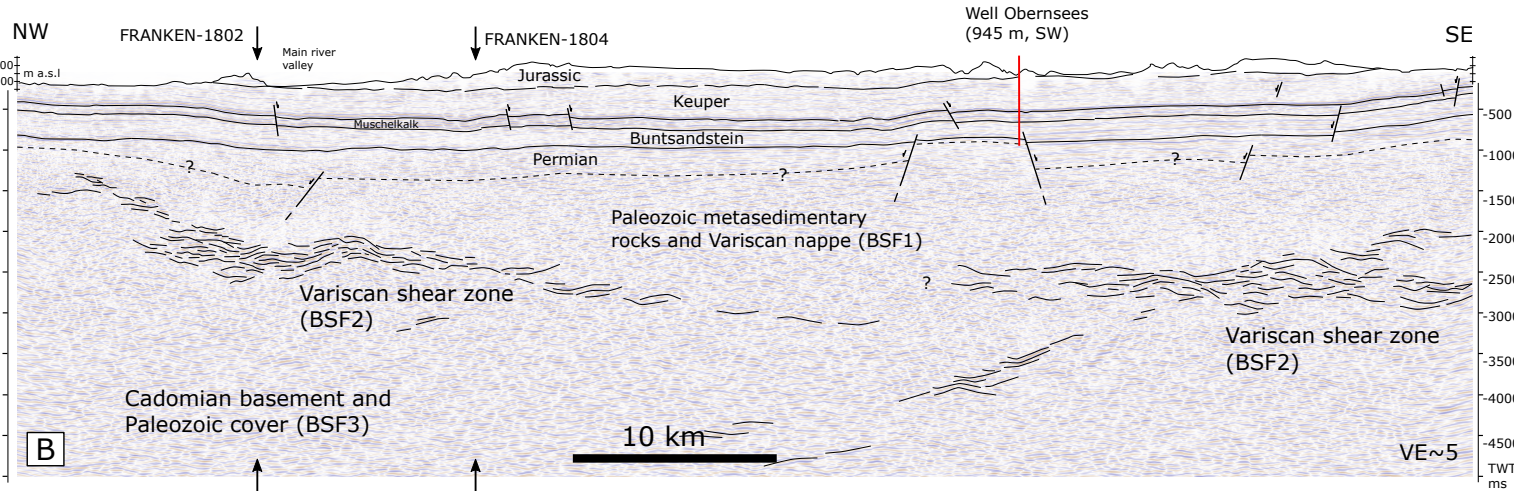
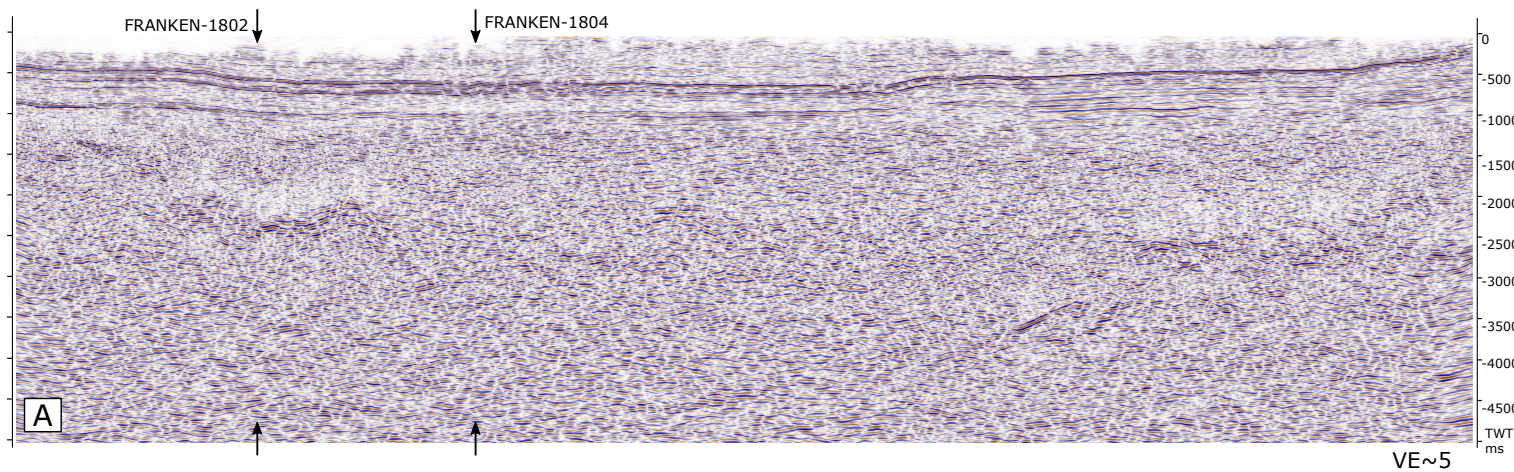


Figure 08

FRANKEN-1804

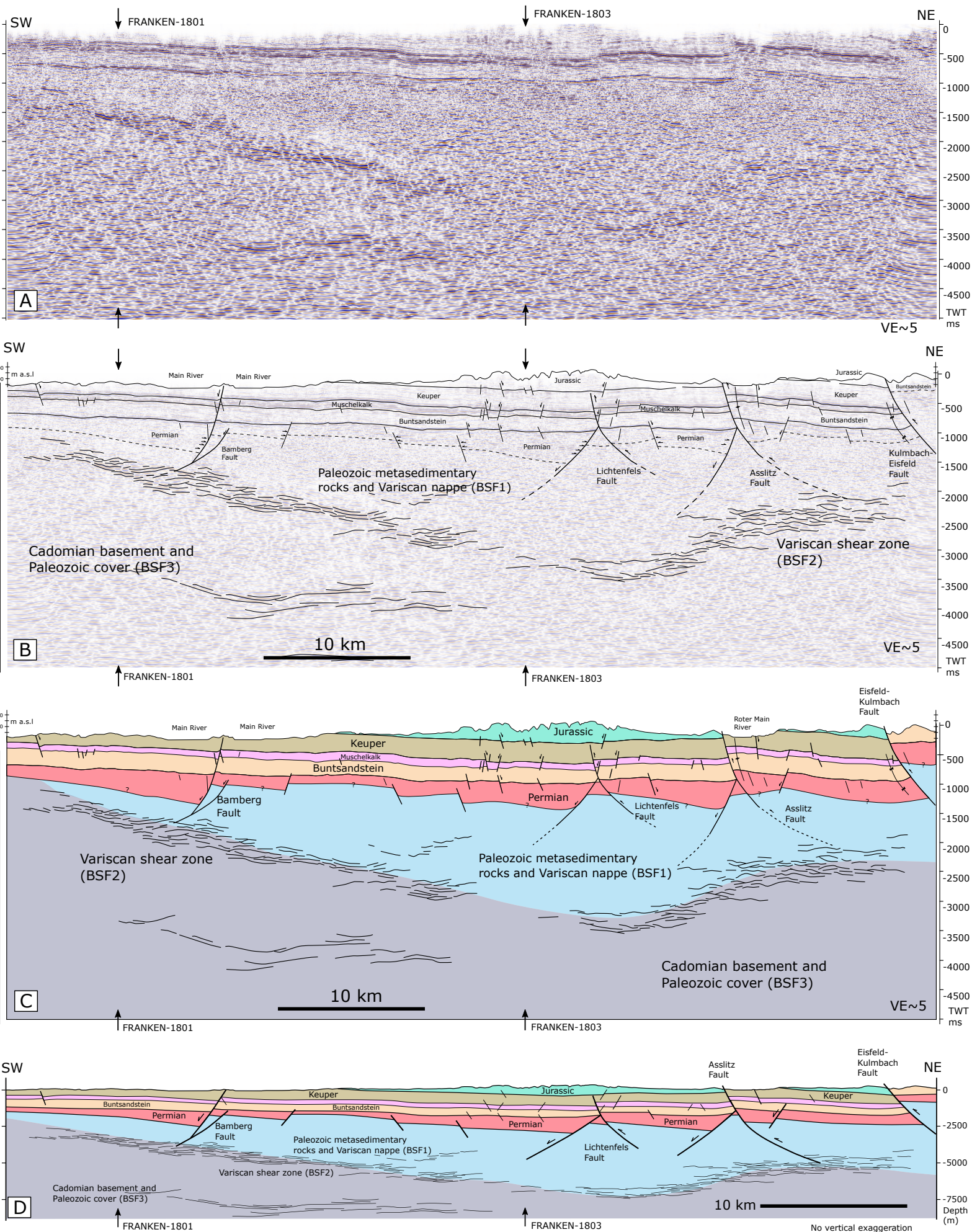


Figure 09

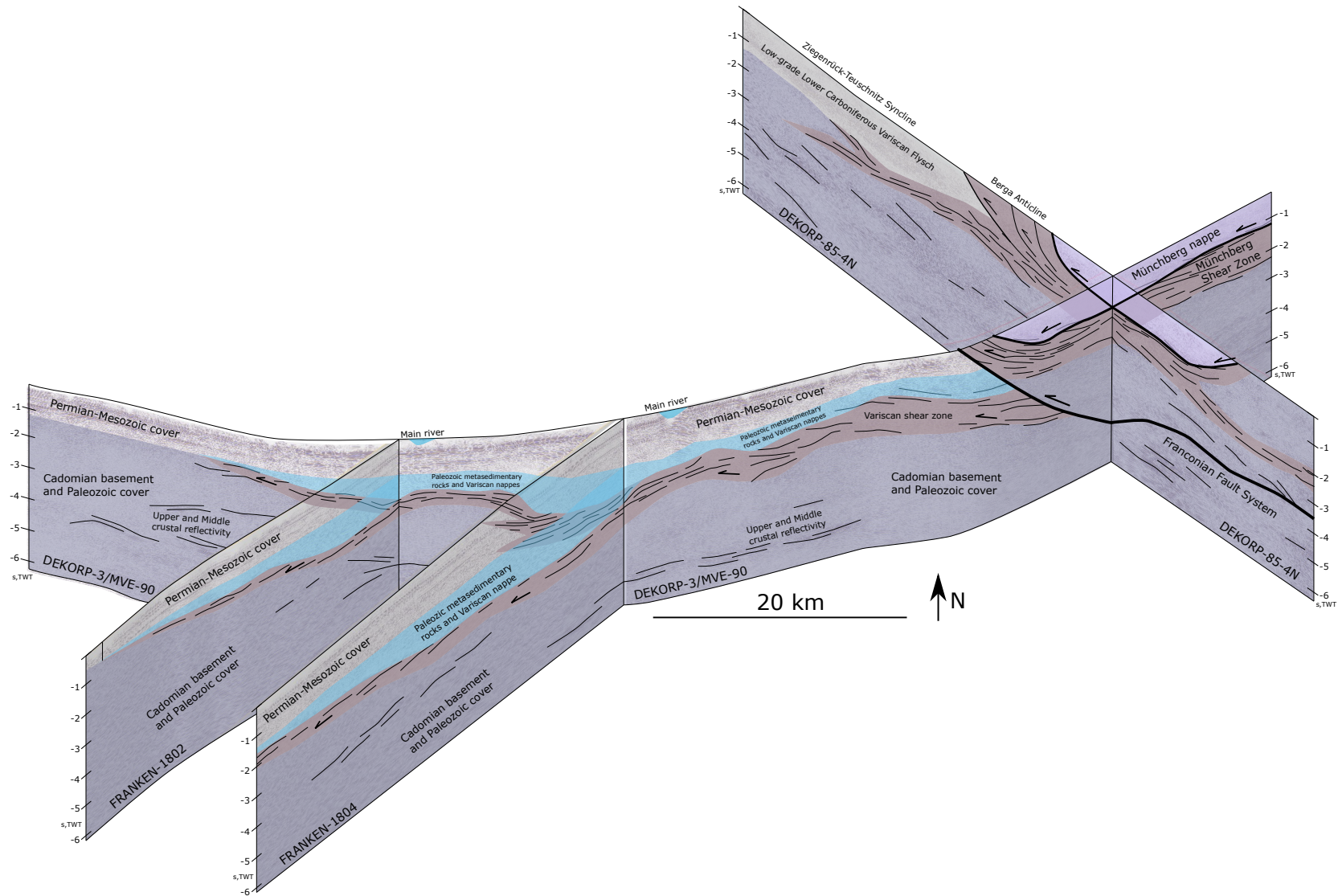
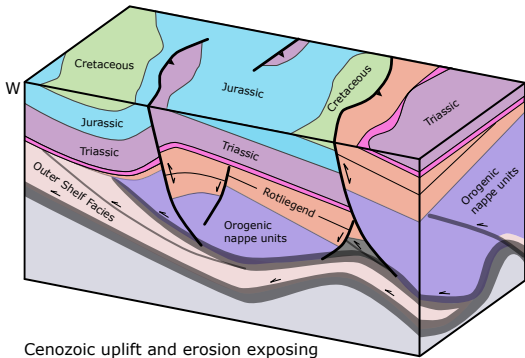


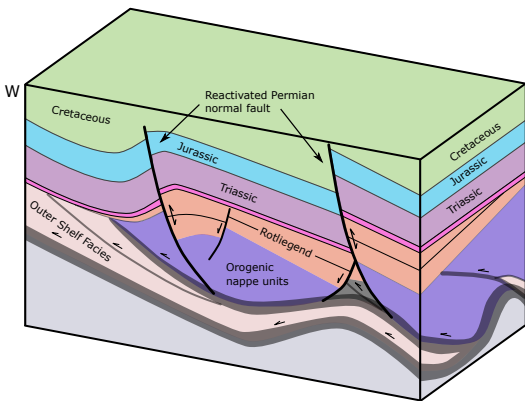
Figure 10

f) Present day



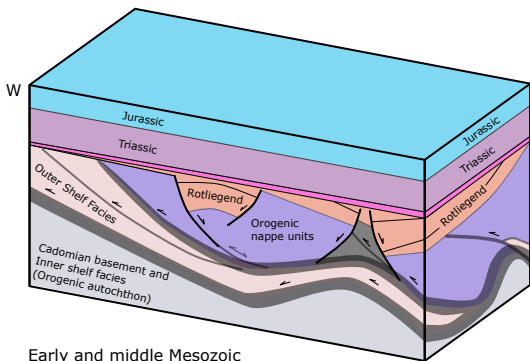
Cenozoic uplift and erosion exposing various stratigraphical levels

e) Cretaceous



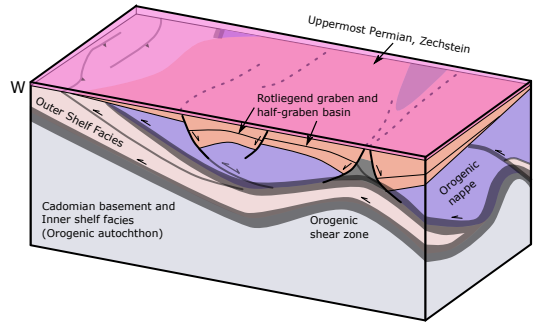
Cretaceous tectonic inversion and selective reverse reactivation of pre-existing (Permian) normal faults

d) Triassic and Jurassic

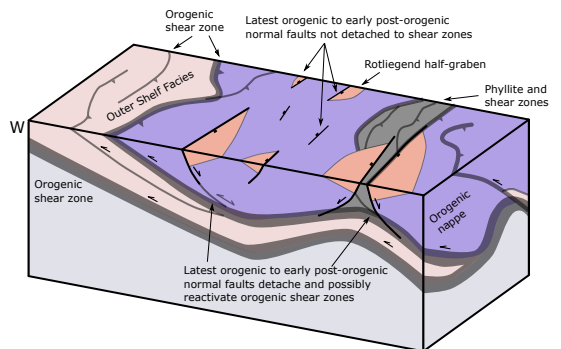


Early and middle Mesozoic regional tectonic quiescence

c) End of Permian



b) Latest Carboniferous-Early Permian



Nucleation and radial propagation of new faults perpendicular to regional stress field. Normal faults sub-parallel to preexisting orogenic shear zone grow while other normal faults eventually abandon.

a) End of orogeny (latest Carboniferous)

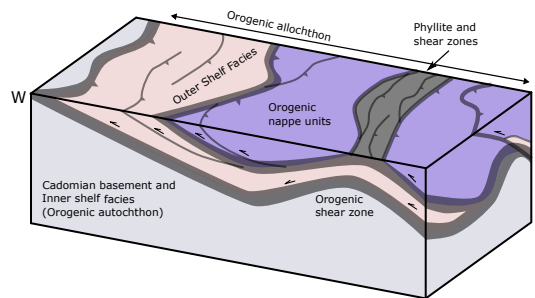


Figure 11

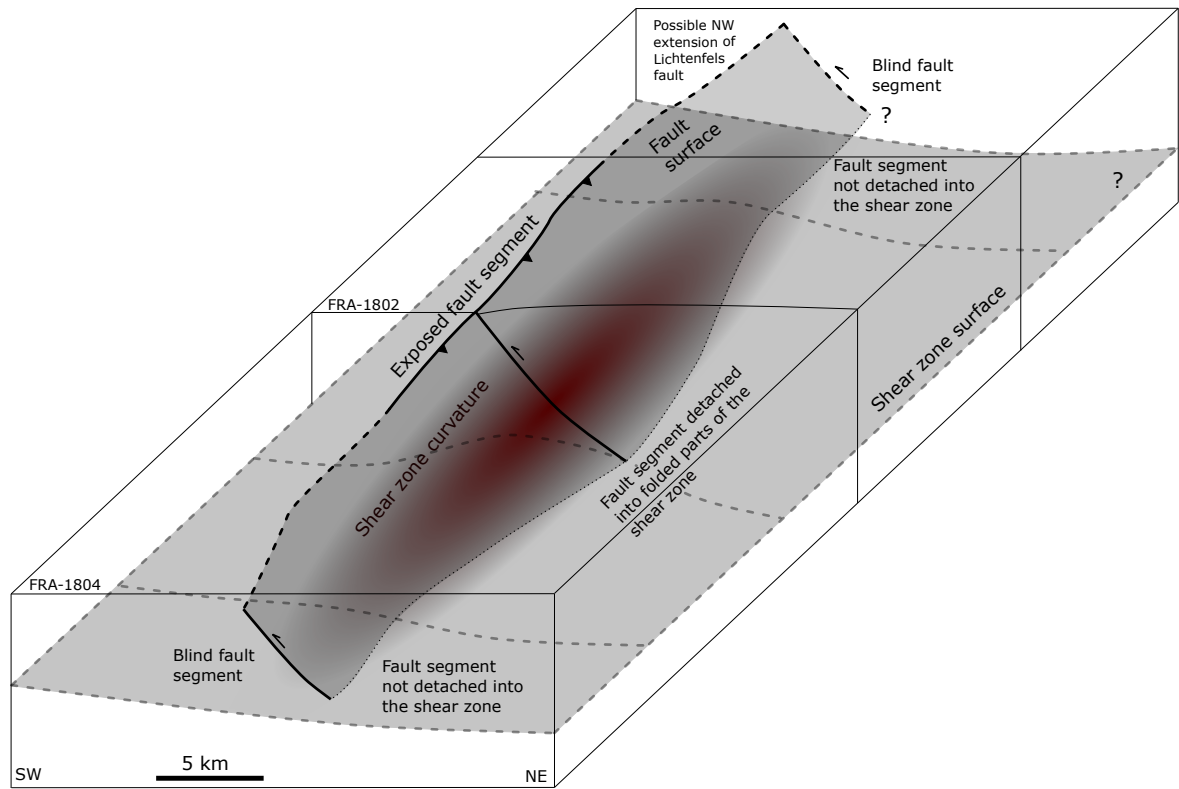


Figure 12

Well	Quaternary	Jurassic	Keuper	Muschelkalk	Buntsandstein	Zechstein	Rotliegend	Basement	TD (m)
Obernsees	0	140	483	178.35	417.15	104.9	18.3	48.3	1390
Mürsbach 01	26	0	300	224	524	126	109	-	1309
Mürsbach 03	0	0	384.4	212.6	551	87	-	-	1235
Mürsbach 04	0	0	345.6	210.5	548.3	73.6	-	-	1178
Mürsbach 05	15.6	0	338.1	214.7	559	56.6	-	-	1184
Mürsbach 06	0	0	338.3	210.7	530.7	121.6	20.7	-	1222
Staffelstein 1	9	102	530.2	239.8	572.2	103.8	43	-	1600
Staffelstein 2	8	104	532	235	301	-	-	-	1180
Eltmann	9.4	0	178.6	235	510	114	3	94	1144
Lindau	0.25	0	0	0	182.05	98.05	250.25	-	530.6
Laineck	3.5	0	409.5	179	488	42	-	-	1122
Haarbrücken	6	0	0	0	199	109.5	185.4	-	499.9
Mittelberg	0	0	0	0	405.5	75.5	41.5	100.5	623
Bad Rodach 1	0	0	130	266	256	-	-	-	652
Bad Rodach 2	0	0	211.7	257.1	526.2	20	-	-	1015
Bad Königshofen	3.5	0	56.5	251	640	76	-	-	1027
Bad Colberg	18	0	322.5	224.5	555.5	157	123.5	-	1401
Wolfersdorf (Stockheim outcrop)	14	0	0	0	0	0	726	29.5	769.5

Table 01

Recording parameters

Number of profiles	4
FRANKEN-1801	47900 m, NW-SE
FRANKEN-1802	47750 m, NE-SW
FRANKEN-1803	71800 m, NW-SE
FRANKEN-1804	63350 m, NE-SW
<hr/>	
Method	Vibroseis
Number of channels	2400
Spread	Symmetrical split-spread with roll-in and roll-off
Active spread	800 stations (2.400 stations) full spread
<hr/>	
Source	
P-wave source	Prakla-Seismos VVCA/E, 3 vibrators
Hydraulic peak force	13.500 da N
Source energy	28.000 lbs / 125 kN (nominal)
Weight	17.000 kg
Sweep length	16.000 ms
Sweep frequency range	8 - 64 Hz
Sweeps per VP	6
Sweep period	8-40 s
Vertical stacking	2 to 4
<hr/>	
Recording	
Source point distance	100 m
Receiver point distance	12.5 m
Natural frequency	10 Hz
Geophone type	Sercel DSU-3, three component MEMS
Recording instrument	Sercel 428 XL
Recording length	8000 ms
Sampling rate	4 ms
Recording format	SEG-D, 8058

Table 02